Aspects of reflectance anisotropy spectroscopy from semiconductor surfaces

1998 J. Phys.: Condens. Matter 10 1

(http://iopscience.iop.org/0953-8984/10/1/005)

J. Phys.: Condens. Matter **10** (1998) 1–43. Printed in the UK PII: S0953-8984(98)78625-4

REVIEW ARTICLE

Aspects of reflectance anisotropy spectroscopy from semiconductor surfaces

Z Sobiesierski†, D I Westwood and C C Matthai

Department of Physics and Astronomy, University of Wales, Cardiff, PO Box 913, Cardiff CF2 3YB, UK

Received 8 August 1997, in final form 20 October 1997

Abstract. There currently exists a wide range of powerful techniques for probing surfaces, mainly involving the use of electron or ion beams under high- or ultra-high-vacuum conditions. Recently there have been major efforts to develop surface sensitive optical probes that have the inherent advantage that they can be applied in more challenging environments such as in high pressures or under liquids and in real time. The most powerful of these techniques to emerge (∼10 years ago) is reflection anisotropy spectroscopy (RAS), which early on demonstrated its ability to distinguish different reconstructions of GaAs(001) and to detect monolayer-growth-related oscillations similar to those routinely obtained using reflection high-energy electron diffraction. This article describes some aspects of the development of the RAS technique since that time, focusing on our own theoretical and experimental studies concerning the (001) surfaces of cubic semiconductors which have been prepared by molecular beam epitaxy. These studies demonstrate that in surface chemistry, structure and electronic properties RAS has made powerful contributions to the study of such surfaces.

Contents

† Author for correspondence. Tel: (+44) 1222 874992. Fax: (+44) 1222 874056. E-mail address: sobiesierski@cf.ac.uk

0953-8984/98/010001+43$19.50

1. Introduction

Surface science has undergone somewhat of a revolution since the late 1980s, both in terms of the local surface structure which can be explored by various scanning probe techniques, and the conditions under which measurements can now routinely be performed. The increasing application of surface-sensitive optical techniques has allowed non-destructive measurements to be made *in situ*, over a broad range of operating environments, and in real time. The techniques which have been applied include surface differential reflectivity (SD), spectroscopic ellipsometry (SE), reflectance anisotropy spectroscopy (RAS), surface photoabsorption (SPA), second-harmonic generation (SHG) and Raman spectroscopy (RS). Whilst each of these approaches has its own individual merit, RAS has proved to date to be the most generally applicable, and successful, of these optical techniques since it combines an ease of use with a high degree of surface sensitivity and an excellent signal-to-noise ratio.

Reflectance anisotropy spectroscopy (RAS) or, as it is sometimes referred to, reflectance difference spectroscopy (RDS) involves the interaction of polarized electromagnetic radiation with the surface (and bulk) electronic dipole moments. With this technique, the difference in reflectance between two orthogonal polarization states of light falling at near-normal incidence on the sample surface is measured. When applied to the surface of an isotropic bulk crystal, e.g. the (001) face of a zincblende semiconductor, there is no net contribution from the bulk to the RAS signal. Under these conditions, the RAS signal arises from a reduction in the surface symmetry, with respect to that of the bulk, caused by surface reconstruction or relaxation.

A number of articles have been published to date describing the evolution and implementation of the RAS technique [1–7] providing details of some of the qualitative and quantitative measurements, such as determining the sample temperature and monitoring surface cleaning procedures *in situ*, which RAS can provide on a routine basis. In one of the most recent of these, Zettler [6] carried out an extended comparison between RAS and spectroscopic ellipsometry (SE).

In this article we intend to focus on our own theoretical calculations and RAS measurements from the (001) surfaces of cubic semiconductors which have been prepared by molecular beam epitaxy (MBE), the growth technique which continues to provide the best characterized surfaces. However, complementary examples drawn from metal–organic vapour phase epitaxy (MOVPE) and chemical beam epitaxy (CBE), in addition to other MBE studies, will be included where appropriate. Unless stated, all of the RAS measurements to which we refer have been carried out *in situ*, under ultra-high-vacuum (UHV) conditions, at the growth temperature. It is not our aim that this article should be an exhaustive review, more that it provides an up to date account of the range of application and the theoretical understanding that it is now possible to attain.

1.1. Experimental considerations for RAS

Reviews of the performance of different forms of RAS system have been made by Aspnes *et al* [2] and Zettler [6]. Aspnes *et al* [2] performed an accuracy analysis for several different possible configurations of reflectance difference (anisotropy) set-ups, and achieved a sensitivity limit of 5×10^{-5}. The experimental system that we have employed for RAS measurements is based on the near-null optical bridge design, developed by Aspnes and co-workers [2], and depicted schematically in figure 1. With this arrangement, the sample is adjusted so that the plane of polarization of the incident beam lies at an angle of 45° to both the [110] and [−110] surface crystallographic directions. The polarization state of the reflected beam is determined by passing it through a photoelastic modulator, followed by an analyser crystal with its axis set at 45° to that of the polarizer. This arrangement has been chosen for its inherent stability, since neither the sample nor the polarizer rotates, as well as its high sensitivity.

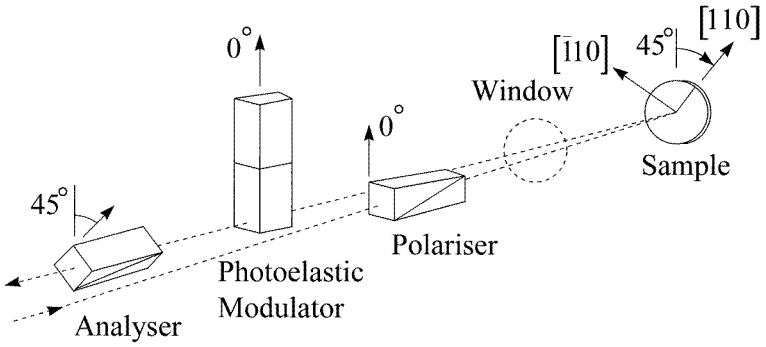

Figure 1. Schematic diagram of the experimental arrangement used for RAS measurements.

The RAS system, which has a working spectral range from 1.5 to 5.5 eV, measures the difference (Δr) between the anisotropic complex reflectance (r) along the [−110] and [110] optical eigenaxes within the (001) surface crystallographic plane, normalized to the mean reflectance ($\bar{r}$).

$$\mathrm{Re}\left(\frac{\Delta r}{\bar{r}}\right) = 2\frac{r[-110] - r[110]}{r[-110] + r[110]}.$$

We have restricted our measurements to only the real part of the RAS signal, since even small residual strain effects, associated with the viewports through which the optical beams pass, significantly affect the imaginary component of the RAS signature [2].

The real part of the RAS signal which we measure can also be related to the surface induced optical anisotropy, $\mathrm{Im}\{(\varepsilon[-110]-\varepsilon([110])d\}$ as described by Zettler [6], i.e.

$$\mathrm{Re}\left(\frac{\Delta r}{\bar{r}}\right)=2\frac{r[-110]-r[110]}{r[-110]+r[110]}=\mathrm{Re}\left\{-\frac{4\pi \mathrm{i}}{\lambda}\left[\frac{(\varepsilon[-110]-\varepsilon[110])d}{\varepsilon-1}\right]\right\}$$
$$=\frac{4\pi}{\lambda}\mathrm{Im}\left\{\frac{(\varepsilon[-110]-\varepsilon[110])}{\varepsilon-1}d\right\}$$

where d is the thickness of the anisotropic surface layer which has complex dielectric functions $\varepsilon[-110]$ and $\varepsilon[110]$ for the given polarizations.

The penetration depths of the incident radiation over the working spectral range, for GaAs, InP and Si (as determined from the reciprocal of the corresponding absorption coefficients at room temperature), are plotted in figure 2 as a function of energy. As expected, the penetration depths $(1/\alpha)$ assume their shortest values at the highest photon energies between 4.0 and 5.5 eV, with the penetration depth for InP being ~40 Å at 4.4 eV. These depths are particularly important when contributions to the RAS spectra arise from beneath the surface, e.g. due to the anisotropy of a buried interface or, as will be shown, due to doping effects or simply to optical interference effects.

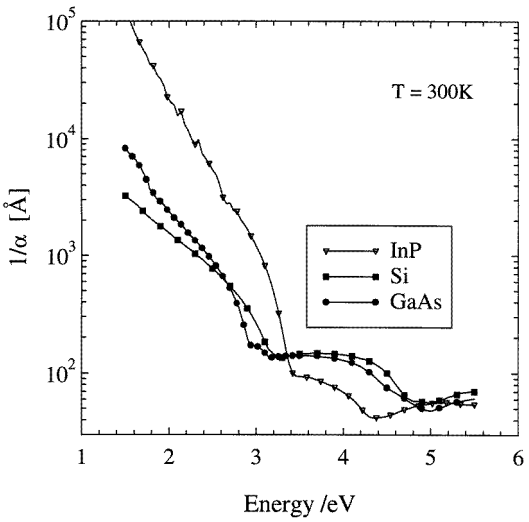

Figure 2. Variation of the penetration depth of incident radiation with energy for GaAs, InP and Si.

1.2. Growth systems employed

Our own results presented in this article were obtained in three separate MBE systems but using the same RAS apparatus. The work on group III arsenides was performed in Cardiff in a conventional solid source VG Semicon V80H reactor using As_4 [8]; the group III phosphide studies were performed in collaboration with the University of Sheffield again in a conventional solid source VG Semicon V80H reactor and using thermally cracked P_2. By contrast the Si(001) studies were carried out in collaboration with the IRC for Semiconductor Materials at Imperial College in a VG Semicon gas source (GS) MBE system using silane and disilane as precursors.

2. Characteristic RAS spectra for semiconductor surfaces

Most of the early RAS work was carried out by Aspnes *et al* [2] on the (001) surface of GaAs, and this still remains the best documented material. Significantly, these authors correlated the RAS spectra with measurements of surface structure, obtained using reflection high-energy electron diffraction (RHEED), for As and Ga stabilizations of the (001) surface of GaAs. This observation, together with that of monolayer oscillations in the RAS signal analogous to RHEED oscillations, demonstrated the immense potential of the technique, especially for environments such as for MOVPE where UHV-based techniques could not be employed. However, interpretation of spectra was and remains difficult, so, for both fundamental and technological reasons, great importance has been attached to the acquisition of spectra representative of different surfaces and reconstructions. To give these spectra meaning they have generally been acquired in MBE systems whose RHEED systems allow the surface structures to be determined.

In addition to GaAs, InP and the ternary alloy $Al_xGa_{1-x}As$ are considered below. Unfortunately there is a clear shortage of characteristic spectra from many of the other important binary (compound) semiconductors (which must form the basis for the subsequent understanding of derivative alloys) often due to a lack of a suitable high-quality substrate material. Frequently materials are grown on alien substrates where the effects of the heterojunction interface, film thickness (including interference effects) and strain may combine to make the acquisition of representative spectra very difficult. For example, RAS data are available for epitaxial layers of AlAs and InAs, grown on GaAs(001). However, whilst the former system is lattice matched to the GaAs substrate, optical interference between the surface and the buried interface becomes important, as is demonstrated in the $Al_xGa_{1-x}As$ section below. The InAs on GaAs(001) system is heavily strained and so even more complicated and is dealt with in detail in section 8. There are also problems with the elemental semiconductors such as Si(001) where, in particular, single atomic height steps lead to multi-domain surfaces with orthogonal dimer bond orientations. This is addressed in a little more detail in section 5.4.

2.1. GaAs(001)

Following the early work of Aspnes *et al*, Wassermeier *et al* [9] extended the GaAs(001) study by comparing RAS spectra with RHEED determined reconstruction, for GaAs(001), over a range of temperatures from 320 to 600 °C. Results from a similar experiment are shown in figure 3 which contains characteristic RAS spectra obtained from our own measurements for GaAs(001), in the temperature range 400–645 °C, using an As_4 stabilizing flux of 5×10^{14} molecules cm^{-2} s^{-1}. The principal change detected in the RAS spectra was that the 2.7 eV minimum, which was present in the spectrum for the c(4×4) surface (an excess As surface), evolved and changed sign to become a local maximum in the RAS spectrum for the (2×4) reconstruction (an As-stabilized surface), indicative of an alteration in surface dimer orientation from along [110] to [−110]. This observation led to the very important conclusion that the 2.7 eV feature arises from surface As–As dimer excitations. More recently Kamiya *et al* [10] carried out the most detailed study for GaAs(001) to date in which both the substrate temperature and As_4 stabilizing flux were varied. From their results, they were able to produce both a surface phase diagram for GaAs and a corresponding database of characteristic RAS spectra for GaAs(001) for the $(2 \times 4)\alpha$, $(2 \times 4)\beta$, $(2 \times 4)\gamma$, c(4×4), d(4×4), (4×2), (3×1), (1×6) and (4×6) reconstructions.

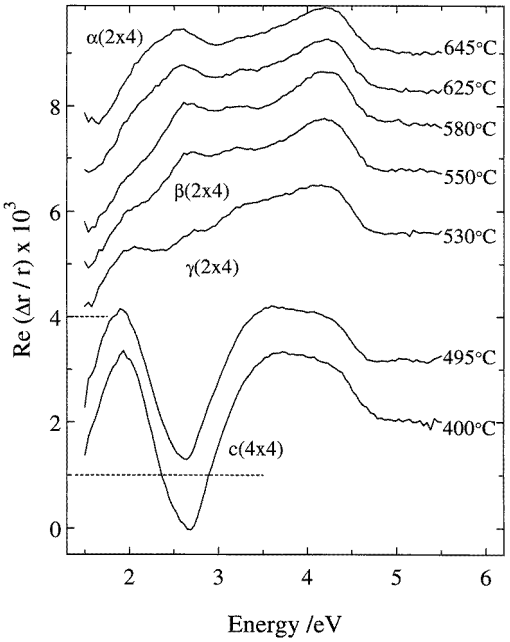

Figure 3. RAS spectra for GaAs(001), where each spectrum has been displaced vertically for clarity. The long/short horizontal dashed lines denote the zero level for the $c(4 \times 4)/\gamma(2 \times 4)$ reconstructions.

Finally, Ploska *et al* [11] have used RAS to compare reconstructions obtained for GaAs(001) under both MOVPE and MBE conditions finding that whilst a (2×4) surface is usually employed in MBE growth, under MOVPE conditions it is dominantly '$c(4 \times 4)$-like'. Time-resolved RAS measurements, obtained at a photon energy of 2.65 eV, showed oscillations with monolayer periodicity for growth with both epitaxial systems. However, the existence of a phase shift between the oscillations obtained for the two systems led the authors to propose different explanations for the existence of growth oscillations under MOVPE and MBE conditions. Further details can be found in section 6, where the use of RAS in monitoring growth and surface morphology are discussed.

2.2. InP(001)

Zorn *et al* [12] have studied InP grown by both MOVPE and CBE (where RHEED was available to determine the surface reconstruction). They concluded that there were only two surface reconstructions which could be obtained under CBE conditions, these being (2×1) for the P-rich surface and (2×4) for the less P-rich surface. However, they noted that other groups had also reported a (4×2) reconstruction under ultra-high-vacuum conditions [13]. The RAS spectra of Zorn *et al* [12] contained a feature at an energy of $\sim$2.8 eV, which could be assigned to P surface dimers, in the same manner as the As-dimer-related feature identified previously for GaAs [9]. In addition to the P-dimer-related feature, the RAS spectrum for the (2×1) reconstruction was found to contain a peak at 3.9 eV, whilst the spectrum for the (2×4) reconstruction contained a minimum at 1.9 eV, plus additional peaks at 3.6 and 4.6 eV.

Recently, Ozanyan *et al* [14] have used a combination of RAS and RHEED to study InP grown by MBE, using elemental In and cracked P_2 sources over a wide range of experimental conditions. Figure 4 shows some results from this study following the evolution of the RAS spectra for static InP(001) surfaces in the temperature range 200–590 °C, with a P_2 stabilizing flux of 3.5×10^{-6} mbar. It is evident that the MBE and CBE results are broadly similar and, by comparison with figure 3, that the range of surface reconstructions which can be obtained for InP(001) are similar to those routinely obtained for GaAs(001). However, it must also be noted [14] that the InP(001)–c(4×4) RHEED patterns are not as distinct as those obtained for the GaAs(001)–c(4×4) reconstruction and indeed the lack of a distinct negative minimum at ∼2.8 eV, as would be expected from the GaAs example, suggests that this reconstruction either does not fully develop or is somewhat different on the InP surface. The full phase diagram from the MBE study, due to Parbrook *et al* [15], where both the P_2 flux and the substrate temperature were varied is shown in figure 5.

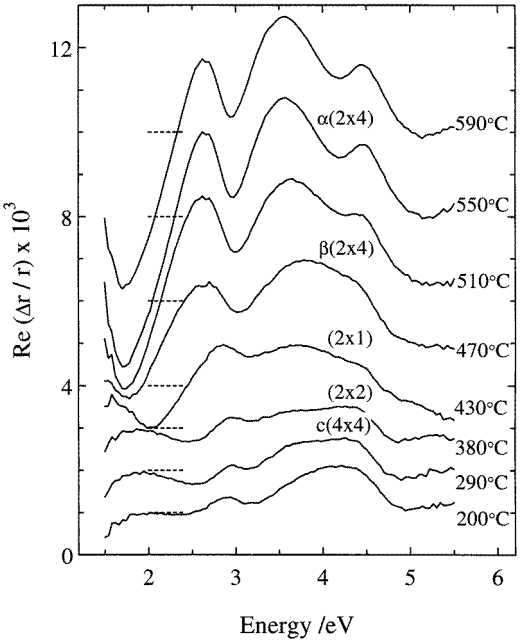

Figure 4. RAS spectra for InP(001), where each spectrum has been displaced vertically for clarity, and the short dashed horizontal lines denote the zero level for each spectrum.

2.3. $Al_xGa_{1-x}As$ on GaAs(001)

Rose *et al* and Morris *et al* [16] have used RAS to study lattice-matched $Al_xGa_{1-x}As$ layers ($x = 0$ to 1.0) grown on GaAs(001). An epilayer thickness of 2.3 μm was finally chosen so as to reduce the contribution of interference fringes to the RAS spectra and so obtain spectra which were representative of bulk $Al_xGa_{1-x}As$ layers. Figure 6 contains RAS spectra for $Al_xGa_{1-x}As$ layers grown on GaAs(001), measured at the growth temperature of 510 °C where they all exhibited a c(4×4) reconstruction. The line shapes and peak energies contained in the spectra for these thick layers all differ from those obtained previously for thin AlAs layers on GaAs(001) [9], indicating that RAS spectra from very thin epilayers

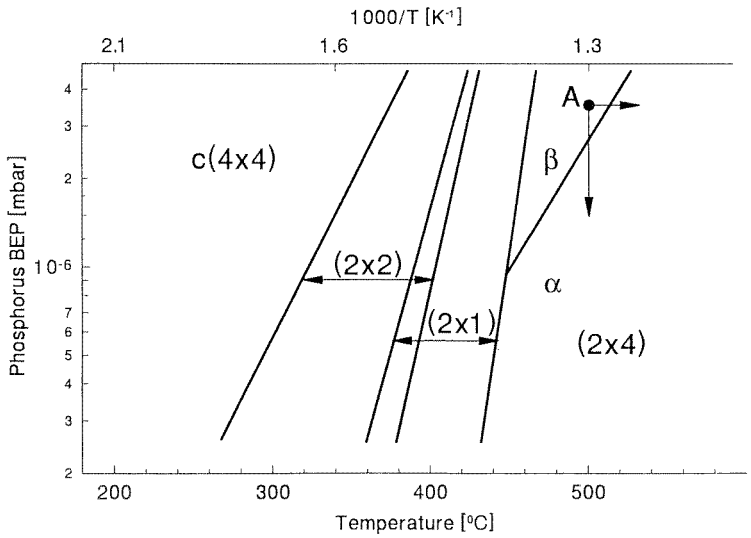

Figure 5. Surface phase diagram for InP(001) (after [14, 15]).

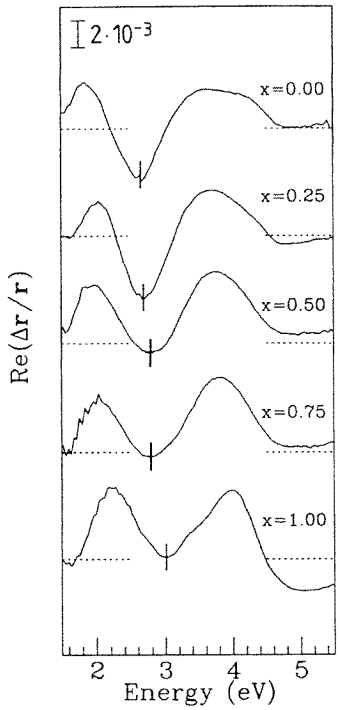

Figure 6. RAS spectra at 510 °C for 2.3 μm thick $Al_xGa_{1-x}As$ layers grown on GaAs(001). The surface reconstruction is c(4 × 4) in all cases (after [16]).

are not truly representative of bulk material. Indeed for very thin films a distinct additional feature appeared at an energy of ∼4.8 eV which, since it did not shift with film thickness,

could not be explained in terms of optical interference and may actually arise from the AlAs/GaAs interface [16]. The positions of the 2.6 eV minimum and the 3.7 eV maximum, which are characteristic features for the clean GaAs(001)–c(4×4) surface in figure 6, both shift to higher energy with increasing Al content. This behaviour appears to be related intuitively to the shift in energy of the bulk energy gaps, E_0 and E_1, with increasing Al content. Such a comparison is made in figure 7, where it can be seen that the RAS 2.6 eV minimum shifts much less, with increasing Al content, than the bulk E_0 ($\Delta E_0 \sim 1.6$ eV) and E_1 ($\Delta E_1 \sim 1.0$ eV) gaps. This indicates that the effect of increasing the proportion of Al atoms is not as large on the surface As dimers as on the underlying atomic layers. The authors of [16] have noted that this is a reasonable expectation for the c(4×4) surface, where the first group III (Ga, Al) atoms appear only in the third layer from the surface. As a final comment, it should be stated that the similarities in the form and the small energetic shifts observed as a function of composition, apparent in figure 6, make it unlikely that RAS spectra can be employed to provide accurate measurements of alloy composition *in situ* during an epitaxial growth process.

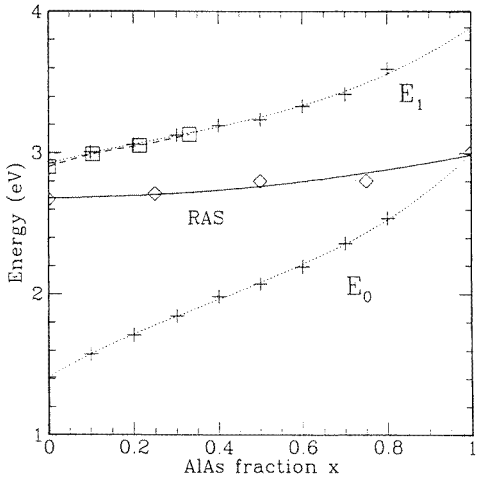

Figure 7. Comparison of the energies of spectral features in the bulk optical spectra and of the minima in the RAS spectra for $Al_xGa_{1-x}As$ layers, as a function of x. The RAS data demonstrate the shift of the 2.6 eV minimum (after [16]).

3. Calculation of the RAS spectra

It has already been shown that the RAS spectra of differently reconstructed semiconductor surfaces, such as of GaAs(001), exhibit particular identifiable features for each structure. Aspnes *et al* demonstrated that some of these features could be associated with the dimer bonds on the surface and their orientation with respect to the polarization of the incident light [1, 2]. Although this simple correlation between one spectral feature and dimer orientation is useful it is of limited value in analysing the host of other surface information apparently provided by RAS. Therefore, to fully exploit this technique, it is important to have a proper understanding of the different factors that influence the RAS spectra. This is best done by performing calculations of spectra from selected, well understood, surface structures and comparing them with experiment. In this way, it is possible to both demonstrate the

viability of such calculations in interpreting RAS spectra and to ascertain the importance of the various approximations that inevitably have to be made in a calculation of this type. The basic structural information necessary for the calculations is obtained from other experimental techniques, especially scanning tunnelling microscopy (STM); however it will become apparent that RAS and STM are actually highly complementary.

3.1. Formulation of the RAS response

The response of the electronic states to electromagnetic fields, which is directly related to the electronic structure, is measured in terms of the dielectric function, ε. There are principally two main contributions to the dielectric constant: an electronic and a lattice contribution. For high frequencies, in comparison to the natural vibrational frequencies of most lattices, which are usually in the infra-red region of the electromagnetic spectrum, the lattice contribution can be neglected. Hence it is possible to obtain a description for the imaginary (absorptive) part of ε at each energy in terms of the density of occupied and empty electron states and of the electron momentum matrix elements.

For large wavelengths compared to the interatomic spacing, the imaginary part of the dielectric matrix can be derived from standard perturbation theory

$$\varepsilon_2 = (e^2/\pi m^2\omega^2)\sum_{cv}\sum_{BZ}\left|\int \mathrm{d}\boldsymbol{r}\psi_c(\boldsymbol{k},\boldsymbol{r})\boldsymbol{e}\cdot\boldsymbol{p}\psi_v(\boldsymbol{k},\boldsymbol{r})\right|^2\delta(E_c(\boldsymbol{k})-E_v(\boldsymbol{k})-\overline{h}\omega)$$

where c refers to an unoccupied conduction band and v to an occupied valence band with energies E_v and E_c respectively. $\boldsymbol{e}$ gives the direction of polarization of the light and $\boldsymbol{p}$ is the momentum operator.

The real part of the dielectric function can be obtained via a Kramers–Kronig transform

$$\varepsilon_1(\omega) = 1 + \frac{2}{\pi}P\int\frac{\omega'\varepsilon_2(\omega')'}{\omega'^2-\omega^2}\,\mathrm{d}\omega'.$$

The dielectric function is related to the real and imaginary parts of the refractive index, n and k respectively, through the relation

$$n + \mathrm{i}k = \sqrt{\varepsilon_1 + \mathrm{i}\varepsilon_2}.$$

The reflectance at normal incidence is then given by

$$r = \frac{1-n-\mathrm{i}k}{1+n+\mathrm{i}k}.$$

The starting point for the calculation of RAS spectra are the wavefunctions obtained from self-consistent *ab initio* pseudopotential or semi-empirical tight-binding electronic structure calculations. Such calculations are usually performed with a slab geometry configuration and so it is important to ensure that the only anisotropy that is calculated is that from the top surface of the slab. This can be done either by using the approach of Manghi *et al* [18] and defining a half-slab polarizability, or by positioning a layer of hydrogen atoms at the bottom surface so that it gives a null contribution to the reflectance anisotropy of the supercell, as in the work of Morris *et al* [19].

3.2. RAS of Si surfaces

The Si(100) (2×1) reconstructed surface has been the subject of much study with some debate over whether the symmetric dimer or buckled dimer model is the correct description of this surface. STM measurements have proved inconclusive and this has been attributed

to time averaging effects. RAS is well suited to provide additional information that could be useful in determining the surface structure. Shkrebtii and Del Sole [20] employed a tight-binding approach to show that the best agreement with the experimental results is obtained by assuming the buckled dimer model. This has been confirmed by the *ab initio* calculations of Kipp *et al* [21] and Kress *et al* [22]. In the latter calculations, it was shown that intra-dimer hopping is less important and the optical matrix elements are mostly determined by hopping through nearby dimers and subsurface orbitals. The presence of the buckling destroys the mirror plane symmetry perpendicular to the dimers, resulting in a lowering of the optical anisotropy and a change in sign. Thus, they were able to show that the anisotropy of the surface-state-related optical peak is very sensitive to the details of the surface reconstruction and of the related charge distribution.

RAS has also been used to study monolayer and submonolayer coverages of As on Si(100) [21] and Sb and Sn on Si(111) surfaces. Kipp *et al* were able to demonstrate that very detailed calculations of the electronic structure and the subsequent optical response does give results that are directly comparable with experimental results [21]. Anyele and Matthai performed self-consistent tight-binding calculations on the structurally similar Sb– and Sn–Si(111) $\sqrt{3} \times \sqrt{3}$ reconstructed surfaces and showed the importance of adatom species on the reflectance anisotropy [23]. In performing these calculations, they were also able to compare the different contributions to the dipole matrix elements. The main finding was that the single-centre integral approximation was quite reasonable for low-energy transitions. Only above 6 eV did the two-centre integrals have a significant effect. The important implication of this is that, in the experimentally measured energy range, the anisotropy spectra are dominated by local optical excitations based on the same site. As these are determined by the local atomic and electronic structure, it may be concluded that RAS does not need a long coherence length of domains and anisotropies resulting from relatively small domains do make a contribution to the measured spectra, in a simple additive fashion.

3.3. RAS of GaAs reconstructed surfaces

Morris *et al* [24] were the first to demonstrate that *ab initio* pseudopotential calculations of the electronic structure and the optical properties, based on the one-electron picture, gave reflection anisotropy spectra that could be compared directly with experimental observations. In a subsequent study of the low-temperature β phase of the GaAs(001) (2×4) reconstructed surface, Morris *et al* [19] showed that a detailed comparison of the calculated and experimental spectra can be used to yield information about the atomic structure of the surface. By calculating the RAS spectrum for the three different structural models (see figure 8) that had been proposed for this reconstruction [25], they found that the experimental spectrum could be interpreted using a linear combination of two structural models for this surface. Thus, the main features of the experimental spectrum, namely the double-hump structure, was best fitted by an 80% contribution from the so-called $\beta 2$ model and 20% from the two-dimer model, as shown in figure 9. The calculated STM images for these two model structures were also found to be in agreement with observations. So in this instance, STM and RAS observations coupled with calculations were able to give information about the surface structure of the GaAs(001) $\beta(2 \times 4)$ reconstructed surface.

Following on from this work, Bass and Matthai turned their attention to the GaAs(001) $c(4 \times 4)$ reconstructed surface [26]. The importance of this reconstruction lies in the fact that it corresponds to the stable As-rich surface and is one of the reconstructions seen in the MBE growth environment. Indeed, RAS growth oscillations have previously been

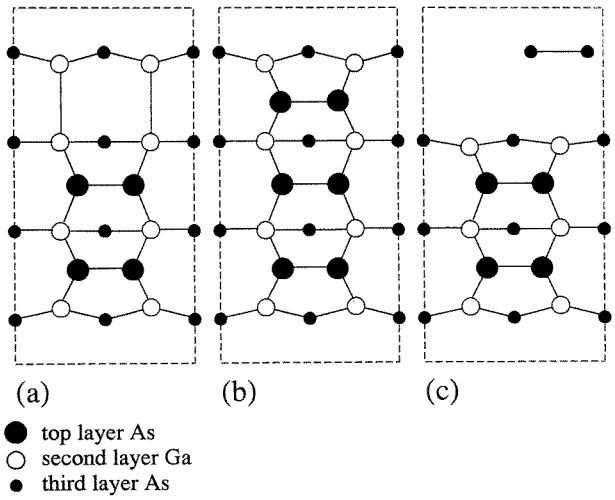

Figure 8. The three models of the GaAs(001)–(2×4) surface for which calculations have been performed. (a) The $\alpha(2 \times 4)$ model with two As dimers in the top layer. (b) The $\beta(2 \times 4)$ model with three As dimers in the top layer. (c) The $\beta 2(2 \times 4)$ model with two As dimers in the top layer and an extra As dimer in the third layer (after [19]).

attributed to an alternating dimer orientation as the growing surface changes between the (2×4) and c(4×4) surfaces. Using the model for the GaAs(001)–c(4×4) surface depicted in figure 10(a), Bass and Matthai were able to obtain excellent agreement with experimental results for this surface. A comparison between the calculated RAS spectrum and the experimental spectrum can be found in figure 10(b). Subsequent analysis of the local density of states for the top layers of the GaAs surface led these authors to deduce that both the main features in the RAS spectrum (the dip at 2.6 eV and the peak at 3.6 eV) have their origins in transitions between very similar *bulklike* valence band states and surface states at two distinct energy levels in the conduction band. The dramatic difference between the (2×4) and c(4×4) signals at $\sim$2.6 eV can then be understood through the energetically lower conduction band state being associated with the directional As–As dimer bonds.

When such highly anisotropic surfaces, such as the GaAs(001)-(2×4) and c(4×4) reconstructed surfaces, have adatom deposits, the RAS spectra show quite marked changes (see sections 4.1 and 4.2). Calculations of the optical response of such surfaces can provide valuable information about the atomic structure. By comparing the experimental spectra with that calculated for different structural models for a 0.25 ML coverage of Si on the GaAs c(4×4), Bass and Matthai [26] were able to demonstrate that RAS could be used to solve for surface structures. It may be noted that they used the same structural models to calculate the STM images indicating the complementarity of the two techniques. In a similar vein, Esser *et al* [27] investigated the microscopic structure of the Sb-stabilized GaAs(001)–(2×4) surface by comparing the observed spectra with that calculated using a tight-binding method for a few plausible surface geometries. Their results indicate a coexistence of Sb and Ga dimers on the Sb-stabilized (2×4) surface.

3.4. Modelling of RAS spectra

From the results of the self-consistent calculations, it may be concluded that the single-particle picture of electron excitations is appropriate for the case of semiconductor structures,

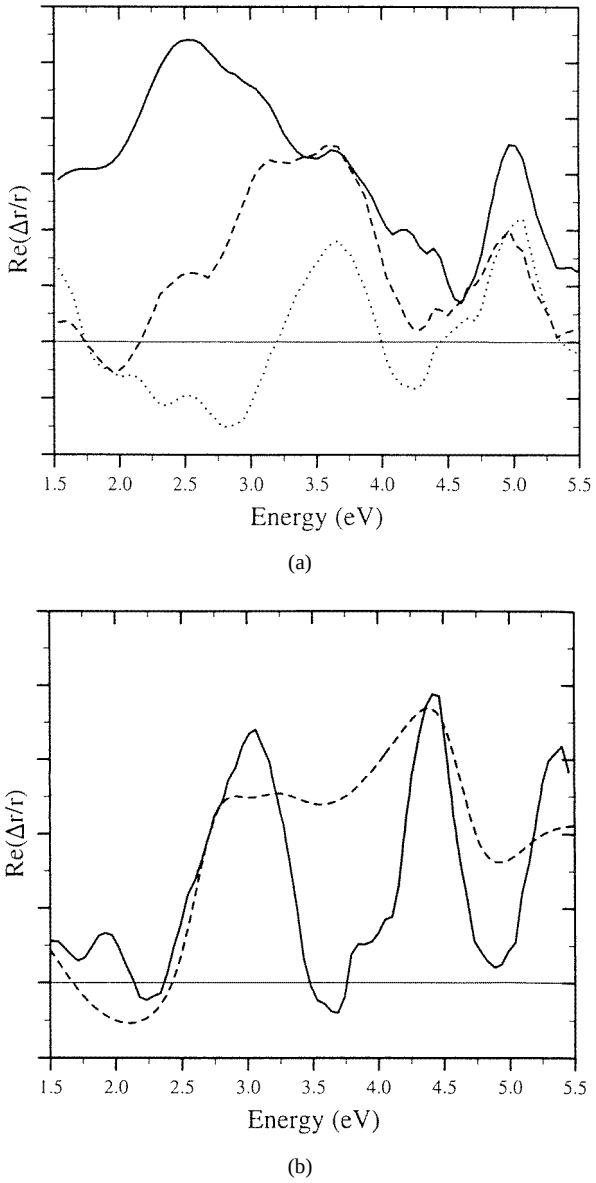

Figure 9. (a) Calculated RAS spectra for the $\alpha(2 \times 4)$ model (solid line), the $\beta(2 \times 4)$ model (dashed line) and the $\beta 2(2 \times 4)$ model (dotted line) and (b) the calculated RAS spectrum (solid line), as obtained from the combination of two structural models, and the low-temperature experimental spectrum (dashed line), for the GaAs(001)–(2×4) reconstructed surface (after [19]).

although, as the surface becomes metallic, it is expected that surface local field effects become increasingly important [28]. The other important consequence of the success of these calculations in reproducing experimental results is that RAS could be used as a surface science tool together with a complementary technique such as STM. However, because RAS is not a diffraction technique and local effects appear to play a predominant role, simple sum rule type arguments can be applied to a surface consisting of several domains

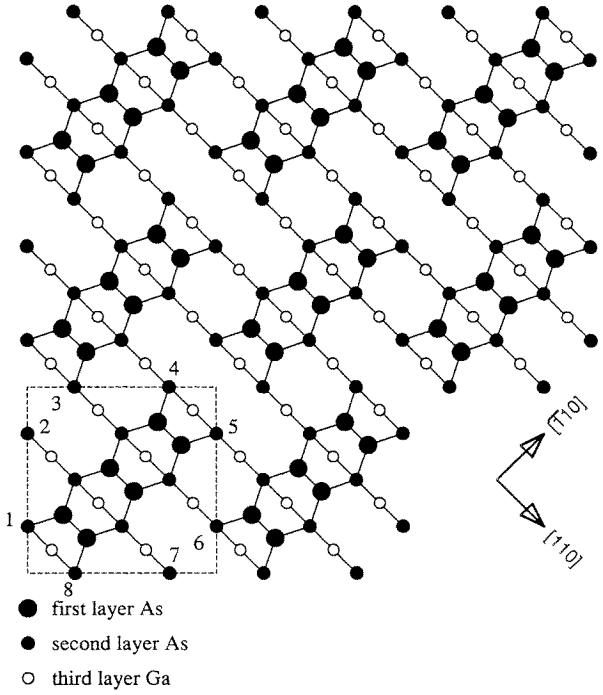

(a)

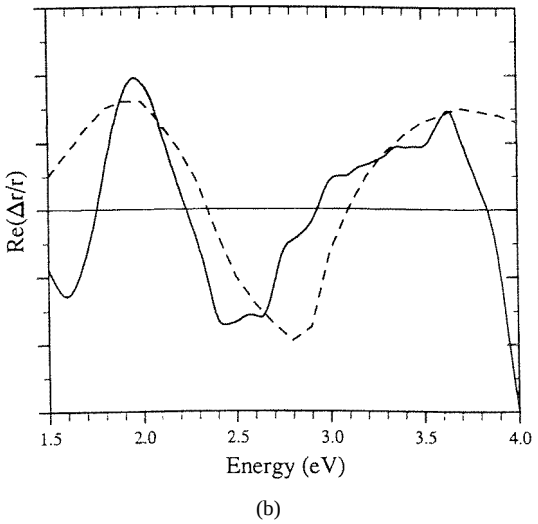

(b)

Figure 10. (a) The model for the GaAs(001)–c(4 × 4) surface and (b) the calculated RAS spectrum (solid line) and the experimental spectrum (dashed line), for the GaAs(001)–c(4 × 4) reconstructed surface (after [26]).

of reconstructions. The measured RAS spectrum is expected to be that of the dominant reconstruction. So, although a real surface may have many defects and imperfections, a calculated RAS spectrum of an idealized surface structure can still be reasonably compared with experiment.

4. Surface science sensitivity

With the early establishment of the ability to distinguish different surface reconstructions and to observe monolayer growth oscillations it was clear that RAS was an extremely surface sensitive technique. However, quantification of this sensitivity remained difficult until the following studies of dopant adatoms on the GaAs(001) surface were performed. This work was part of a wider study examining the concept of delta doping and it should be noted that calculations of Si/GaAs(001) structures have already been briefly introduced in section 3.3, whilst overgrowth of the Si/GaAs(001) structure to form a true δ-doping structure is considered in section 6.4 and the whole of section 7 is devoted to the influence of doping on RAS signals.

4.1. Deposition of Si on GaAs(001)

The synthesis of GaAs-based semiconductor structures employing spatially confined n- and p-type dopants, such as Si and Be, in the form of δ-layers is of considerable scientific and technological interest. In order that such structures may be utilized to their full potential, a detailed understanding is required of the way in which the GaAs surface reconstructions become altered after planes of dopant atoms, such as Si or Be, are deposited on the GaAs surface. The majority of experimental studies have employed either RHEED or scanning tunnelling microscopy (STM) as tools to probe the different surface reconstructions and the details of their atomic bonding [29, 30]. Although these investigations have explored a wide manifold of possible reconstructions, using a broad range of growth conditions, only a small number of studies have been aimed specifically at probably the most technologically relevant Si/GaAs interfaces, i.e. those prepared at low temperature (400 °C and below) [31–33] in order to reduce diffusion and segregation effects.

A combination of RAS and RHEED measurements have been used recently to study sub-monolayer (ML) coverages of Si on the GaAs(001)–c(4×4) surface, at a substrate temperature of 400 °C [31, 34]. Figure 11 contains RAS spectra for the clean GaAs(001)–c(4×4) surface, and following deposition of increasing amounts of Si. On depositing Si (0–0.08 ML) the reconstruction, as determined by RHEED, evolves from c(4×4) to a mixed c$(4 \times 4)/(1 \times 2)$. The surface sensitivity of the RAS technique is demonstrated, dramatically, in this figure by the ability to detect Si coverages as low as 0.005 ML. It is to be noted that there appear to be three 'nodal' or isoplethtic points, at energies of 1.6, 2.3 and 3.1 eV. The way in which the spectra all pass through these three points strongly suggests that each spectrum is, in fact, a superposition of two separate functions, one representing the clean GaAs(001)–c(4×4) surface and the other contribution arising from the evolving (1×2) structure, identified in RHEED measurements. The negative RAS signal at $\sim$2.7 eV for the GaAs c(4×4) surface arises from As–As surface bonds which are aligned in the [110] direction. Hence, the change in amplitude of the 2.7 eV signal, with increasing Si coverage, may be associated with a disruption of the original [110] oriented As–As bonds and the formation of Si–Si bonds aligned along $[-110]$.

It is worth noting that the c(4×4) component of the RAS signal persists at Si coverages much greater than those at which the c(4×4) contribution vanishes in RHEED observations. This may be due to the fact that whereas RHEED, with a typical coherence length of $\sim$2000 Å, is sensitive to long-range order the RAS response, being dependent upon the dimer orientation of the surface species, is more strongly influenced by short-range order, resulting in a coherence length of a few tens of Å (see section 3 and [10]).

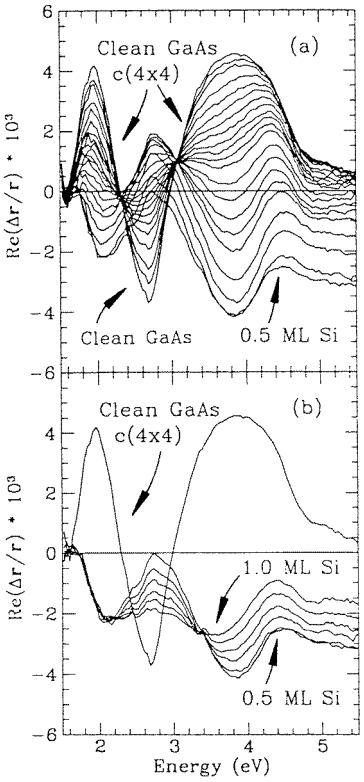

Figure 11. RAS spectra for the growth of Si/GaAs(001). (a) 0, 0.005, 0.01 to 0.10 ML Si (increments of 0.01 ML), 0.12 to 0.20 ML Si (increments of 0.02 ML), 0.25, 0.30, 0.40 and 0.50 ML. (b) 0 ML Si (for comparison), 0.50 to 1.00 ML Si (increments of 0.1 ML) (after [34]).

4.2. Deposition of Be on GaAs(001)

Figure 12 contains RAS spectra following the deposition of Be on GaAs(001), for coverages of (a) 0–0.5 ML Be, and (b) 0.5–1.0 ML Be [34]. As with the case of Si/GaAs, it was possible to detect an overlayer coverage of only 0.005 ML Be. RHEED measurements taken in conjunction with the RAS spectra showed that in this case the starting GaAs(001)–c(4×4) reconstruction altered, via mixed c$(4\times4)/(1\times2)$, c$(4\times4)/(1\times3)$ and $(1\times2)/(1\times3)$ phases, into a (1×3) structure at 0.20 ML Be. For Be coverages less than 0.3 ML, the development of the RAS signatures at photon energies below 3.2 eV was similar to that observed for Si/GaAs, with the existence of nodal points in the spectra at energies of 1.6, 2.4 and 3.2 eV. However, at photon energies greater than 3.2 eV, the evolution of the RAS lineshape for Be/GaAs was different from the Si/GaAs case. Here, the magnitude of the maximum feature at 3.8 eV, for Be/GaAs, both increased and shifted towards a higher energy value for each consecutive Be deposition, such that with a Be coverage of 1 ML the maximum amplitude of the RAS spectrum was nearly double that of the original GaAs(001)–c(4×4) spectrum. The reason for the difference in sign of the RAS signal for the Si and Be/GaAs spectra above 3.2 eV is not yet fully understood; although it may be related to the fact that Si and Be are dopant species of opposite type in GaAs.

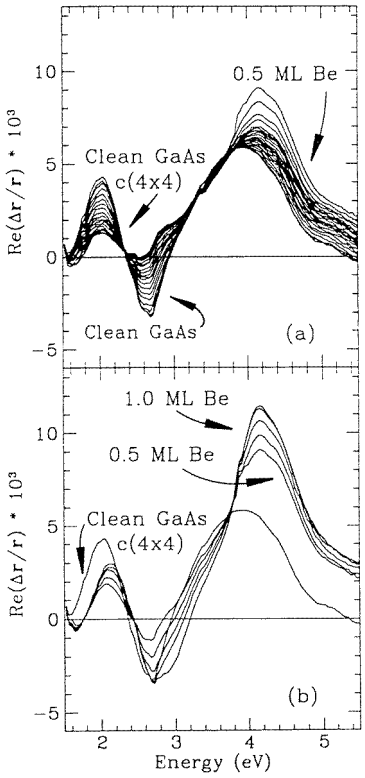

Figure 12. RAS spectra for the growth of Be/GaAs(001). (a) 0, 0.005, 0.01 to 0.10 ML Be (increments of 0.01 ML), 0.12 to 0.20 ML Be (increments of 0.02 ML), 0.25, 0.30, 0.40 and 0.50 ML. (b) 0 ML Be (for comparison), 0.50 to 1.00 ML Be (increments of 0.1 ML) (after [34]).

5. Studying the surface chemistry

Whilst previous sections have largely established the nature of the RAS technique, the remainder of the article is concerned with addressing its different areas of application in more detail. The first of these is 'surface chemistry' where the high surface sensitivity and the dependence on adatom species make RAS a potentially very important technique. In addition, another consideration is the rate of reaction and this is usually addressed by acquiring data in real time, at a fixed photon energy. This photon energy is usually chosen based on the results of spectroscopic 'surveys'.

5.1. Oxide removal from InP surfaces

The majority of common substrate materials, e.g. Si, GaAs and InP, undergo some form of wet chemical etching, prior to loading into a growth reactor. In all cases, this process is designed to leave the substrate covered in a protective oxide layer, which is easy to desorb by heating. After thermal removal of the oxide, the semiconductor surface is clean, reconstructed and ready for the subsequent deposition of epitaxial material. Figure 13 contains real-time optical transients taken during the thermal deoxidation of the thin InP oxide layer obtained after etching with an H_2SO_4:H_2O_2:H_2O solution, from the work of

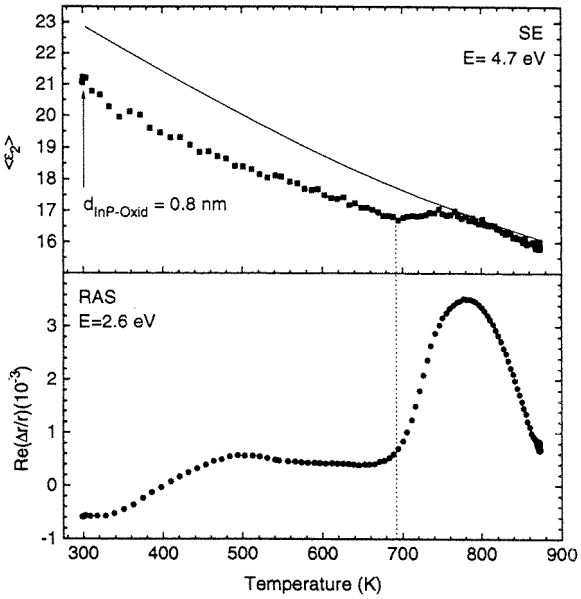

Figure 13. Deoxidation transients for spectroscopic ellipsometry (SE) and RAS of wet-chemically etched InP wafer (after [35]).

Knorr *et al* [35]. The photon energies of the RAS and SE transients were chosen to be 2.6 eV and 4.7 eV, respectively. At these energies, the transients are sensitive to the P-dimer formation (RAS), and the oxide overlayer thickness (SE). During oxide desorption, the surface was stabilized with phosphine, under standard MOVPE conditions. The temperature was ramped in about 7 min from room temperature to the final growth temperature. With increasing temperature, the SE signal decreases until the oxide starts to desorb at around 693 K. The corresponding RAS dataset shows a large increase in intensity at the temperatures for which oxide desorption becomes significant. This sudden increase in RAS signal is due to the appearance of a reconstructed InP surface. At still higher temperatures, the signal decreases due to the thermal downshift of the P-dimer-related RAS peak.

5.2. As/P exchange reaction on InP(001)

The exchange of group V atoms on the surface of a III–V semiconductor can affect both the interface properties and thickness of quantum structures. In MBE, the desorption of the surface oxide from InP substrates is often carried out under a stabilizing As flux in order to avoid the use of phosphorus [36]. Oxide removal under As stabilization of the InP surface results in the exchange of P for As atoms, leading to the formation of a thin pseudomorphic InAs layer on the InP surface [37, 38]. The structural properties of such InAs layers have been investigated in some detail [38], with a consensus being reached that the InAs surface layer invariably stabilizes at a thickness of two monolayers, with very little As incorporation beyond the second monolayer from the surface. Moreover, the InAs/InP interface thus formed is of sufficient quality to allow efficient carrier capture and radiative recombination within the InAs/InP surface quantum well [39]. Hence, the exposure of the InP surface to an As flux suggests itself as a highly appropriate system with which to study the kinetics of the As/P exchange reaction.

In situ optical probes have been used to investigate the kinetics of As/P exchange on InP(001) under MOVPE conditions [40], as well as As capture by InP(001) surfaces under CBE conditions [41]. In the first case [40], surface photo-absorption (SPA) at 470 nm was used to monitor the change in surface reflectivity on exposure of the InP(001) surface to AsH_3. An activation energy of 1.26 eV was obtained for As/P exchange based on various assumptions, including the fact that only a single monolayer is affected by the exchange process. In addition to being limited to a fixed wavelength, it has been noted [42, 43] that this study was performed on the group-III-terminated (In) surface, a somewhat unusual condition for conventional epitaxial growth.

Recently, RAS has also been applied in this area and data obtained from P-stabilized InP(001) surfaces exposed to As, under MBE conditions, using solid sources for In, cracked As (As_2) and P (P_2) [44]. Following thermal desorption of the surface oxide under a P_2 pressure of 3.5×10^{-6} mbar, a 0.5 μm InP buffer was grown at 510 °C. RAS spectra were subsequently acquired for static (i.e. no growth) surfaces before, during and after As_2 exposure, in the presence of the P_2 flux. RAS transients, monitored at an energy of 2.65 eV (peak energy of a feature related to surface As–As bonds), were also recorded during the initial exposure and final removal of the As_2 flux.

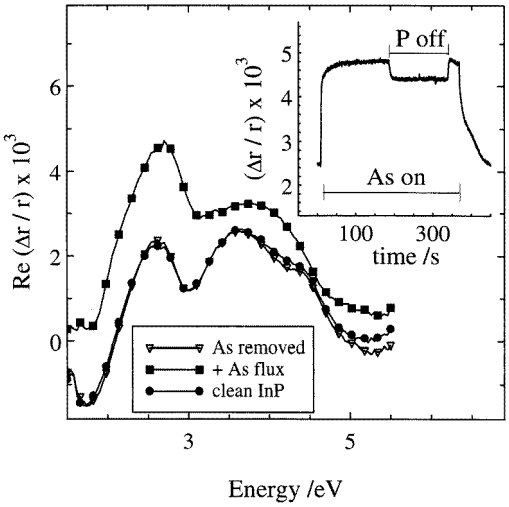

Figure 14. RAS spectra measured at 510 °C for InP(001) before (●), during (■) and after (▽) exposure to an As_2 flux of 4.6×10^{-6} mbar. The inset shows a time-resolved measurement performed at 2.65 eV during a similar sequence (after [44]).

Figure 14 displays the RAS spectra obtained at 510 °C before, during and after exposure of the InP(001) surface to a 4.6×10^{-6} mbar As_2 flux. Sufficient time was allowed (∼3 min) for the surface to stabilize, in each case. The peak located at 2.65 eV for the clean InP surface remains at approximately the same energy following As_2 exposure, rather than shifting to 2.3 eV, the energy characteristic of bulk InAs. This behaviour is fully consistent with the formation of a very thin InAs layer, pseudomorphically matched to the InP substrate, and it should be noted that similar spectra have also been observed for thin InAs layers (<10 ML) grown on InP(001). The overall similarity in shape between the RAS spectra for the clean and As-exposed InP surfaces indicates that the surface symmetry remains essentially unaltered during the exchange process. This observation has been verified by

RHEED measurements, taken simultaneously during As_2 exposure, which reveal that the reconstruction is (2×4). By performing separate measurements, using incrementally larger As_2 fluxes, it has been possible to establish that exposure to an As_2 flux of 4.6×10^{-6} mbar provides the greatest change in RAS response, at this temperature. In this respect, it will be referred to subsequently as the 'optimal' flux.

Since the largest spectral change following As_2 exposure occurs around 2.65 eV, the energy characteristic of surface dimer species, this energy has been used to monitor the temporal behaviour during the As/P exchange process. The inset to figure 14 shows a time-resolved measurement of the RAS intensity at 2.65 eV before, during and after As_2 exposure. In addition to the transients obtained at the start and end of As_2 supply to the surface, it can be seen that the signal also decreases when the P_2 flux is turned off. Similar behaviour can also be obtained, in the presence of P_2, by increasing the As_2 flux above the 'optimal' level of 4.6×10^{-6} mbar described previously. This indicates a complicated dependence on the total group V flux and has yet to be fully investigated.

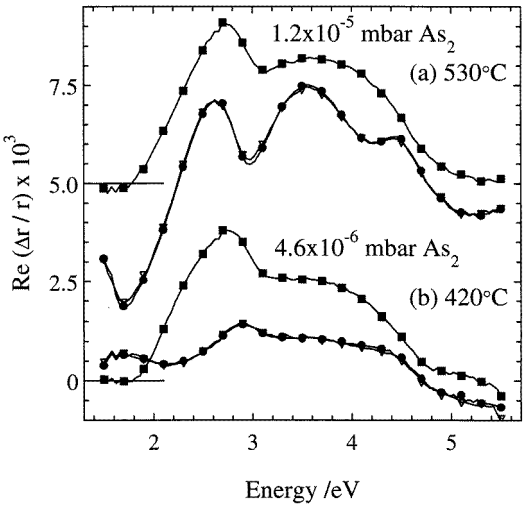

Figure 15. RAS spectra measured at (a) 530 °C, and (b) 420 °C, for InP(001) before (●), during (■) and after (▽) exposure to As_2 fluxes of 1.2×10^{-5} and 2.8×10^{-6} mbar, respectively. The horizontal lines indicate the corresponding 'zero' levels for the two sets of spectra (after [44]).

Figure 15 contains similar sequences of spectra obtained at temperatures of (a) 530 °C and (b) 420 °C, with 'optimal' As_2 fluxes of 1.2×10^{-5} and 2.8×10^{-6} mbar, respectively. The InP(001) reconstruction for the clean, P-stabilized, surface was found to alter from (2×4) at 530 °C to (2×2) at 420 °C. The data in figure 15 show clearly that the As/P exchange reaction is fully reversible over a range of temperatures from 420 °C to 530 °C. In fact, RAS measurements performed at temperatures as high as 560 °C show a similar degree of reproducibility between the spectrum obtained for the clean InP(001) surface and the spectrum following application and removal of the As_2 flux. However, at this elevated temperature it has not been possible to supply enough As_2 to maximize the spectral change observed for the As-exposed surface. This is probably due to the high evaporation rate for As from the surface at 560 °C.

Finally, RAS transients, monitored at an energy of 2.65 eV during As_2 exposure, have been acquired over the entire temperature range studied. The time taken for the change in intensity to reach 95% of its maximum value has been determined, and the reaction rate

has been defined as the reciprocal of this quantity [44]. Figure 16 shows an Arrhenius plot of the natural logarithm of the reaction rate versus reciprocal temperature. The activation energy for As/P exchange on InP(001) obtained in this manner is 1.23 ± 0.05 eV. This can be compared directly with a value of 1.26 eV obtained from SPA measurements on the In-rich InP surface, using a much narrower range of temperatures from 370 to 400 °C, under MOVPE conditions [40]. It may also be compared with a separate RAS study of P/As exchange for GaAs(001) exposed to PH_3 [42, 43] where the activation energy was determined to be 1.64 eV.

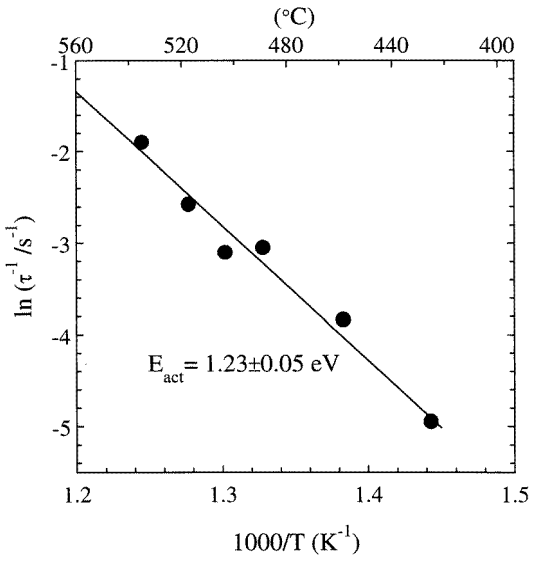

Figure 16. Natural logarithm of the rate constant for As/P exchange (as determined from the RAS transients on As exposure to InP(001)) against reciprocal temperature (after [44]).

5.3. Exposure to hydrogen

For III–V semiconductors, exposure to atomic hydrogen is known to break surface dimers and to saturate the dangling bonds at the surface. Esser *et al* [45] have used RAS, SE and LEED to investigate the hydrogen-induced modification of the surface structure and dielectric properties of GaAs(001)–c(4×4), (2×4) and (4×2) reconstructions. For low H exposures, the removal of surface dimers results in a decrease of the RAS signal, whereas for larger H exposures, the RAS signal increases once again in response to the anisotropic surface etching which generates rough GaAs surfaces.

In comparison, the surfaces of H-terminated elemental group IV semiconductors, such as Si or Ge, are far more chemically inert. This means that they are very reliable and reproducible systems to perform RAS measurements on. The first investigations on H- and SiO_2-terminated Si surfaces were carried out by Yasuda *et al* [46], where the hydrogen passivation was achieved through wet chemical treatment using hydrofluoric acid. The RAS spectra for Si–SiO_2, following correction of oxide thickness artifacts [47], were found to be not substantially different to those from the H-terminated Si surfaces. Further studies of clean, single-domain, Si(001) and Ge(001) surfaces not only allowed the influence of exposure to oxygen to be studied, but also provided RAS spectra for comparison with

theoretical calculations [48]. It is these measurements, and subsequent developments, which we shall discuss in more detail here.

It has been shown that clean Si(001) surfaces, at room temperature, form asymmetric dimers that are parallel to each other within a given terrace [49]. For a singular surface, adjacent terraces, separated by single atomic height steps, form dimer domains rotated by 90° relative to each other. Therefore, the surface contains both (2×1) and (1×2) reconstructed domains, which occupy approximately equal areas, and hence there is no net contribution to the RAS response. However, for vicinal surfaces, e.g. Si(001) misoriented by 4° in the [110] direction, the clean surface is dominated by double-height steps, so that dimers in adjacent terraces run parallel to each other [50]. In this case, there are STM data which suggest that clean Si(001)4°–[110] surfaces are largely single domain, (2×1), with a minority (1×2) domain coverage of ∼15% at room temperature [51]. Figure 17 contains RAS spectra obtained from clean, vicinal Si(001) surfaces in the temperature range 350 to 750 °C. It can be seen that whilst the overall shape of the spectrum remains unaltered, the intensity at 4.25 eV decreases with increasing temperature. Cole *et al* [52] have used the variation in RAS intensity, at this photon energy, as a monitor of the Si(001)–(1×2) minority domain coverage, and this has been found to vary from ∼15% at room temperature to ∼40% at 750 °C. However, for photon energies below 3.4 eV (the E_1 energy gap for Si) no systematic variation in RAS intensity with temperature has been observed.

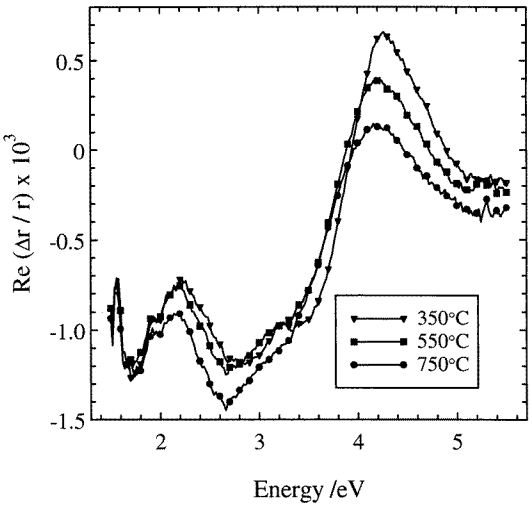

Figure 17. RAS spectra taken for clean, static (no growth) vicinal Si surfaces, for temperatures from 350–750 °C.

Yasuda *et al* [48] used a combination of RAS and LEED measurements to study the exposure of clean vicinal Si(001) surfaces to oxygen. However, it was surmized that the thermal processing used to clean the Si resulted in the surface reconstruction becoming monohydride (2×1), following H contamination. As a result, the surface dimers were found to be resistant to oxidation, and the initial change in RAS signal upon exposure to oxygen was attributed to surface steps. The idea that the RAS signal for group IV surfaces arises from a linear combination of step and terrace contributions has been developed further by Rossow *et al* [53]. These authors have concluded that both hydrogenated and oxidized surfaces show derivative-like RAS lineshapes, which arise from bulk critical points that

have become dichroic, as a result of a potential which arises either from chemical change or strain at the surface. In contrast, the RAS lineshapes for clean surfaces are believed to be dielectric-function-like and contain only minor contributions from steps.

5.4. Hydrogen desorption from vicinal Si(001) surfaces

The growth of Si by gas-source MBE, using disilane (Si_2H_6), has been studied using a combination of RHEED and RAS measurements by Turner *et al* [54], and Zhang *et al* [55]. Changes in the relative domain coverage of the (1×2) and (2×1) surface reconstructions, for growth on singular substrates, have been shown to result in oscillations in the RAS intensity which occur with twice the period of the RHEED intensity oscillations [55]. These RAS oscillations have only been observed for growth temperatures between 550 and 650 °C. In order to study surface hydrogen coverage during exposure to disilane (Si_2H_6) which, through pyrolysis, may also result in growth, it is necessary to eliminate these domain coverage induced variations. To achieve this we have used vicinal Si(001) substrates, misoriented by 4° in the [011] direction to provide a dominant domain (ratio 1:3 at 550 °C [52]), through the formation of double-height steps. In addition, due to the small terrace width on this surface it is found that growth occurs by step flow and so does not contribute any change to the RAS signal. This is evidenced by the lack of RAS oscillations for growth on vicinal Si(001) surfaces [55].

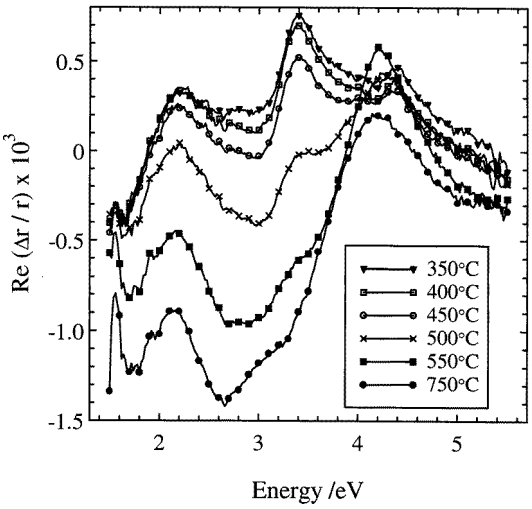

Figure 18. RAS spectra acquired during disilane growth on vicinal Si(001), in the temperature range 350–750 °C.

Figure 18 shows a series of RAS spectra taken during disilane exposure, in the temperature range 350–750 °C. In this case, the large change observed in the RAS signal for photon energies below the E_1 threshold at 3.1 eV is consistent with the removal of the Si dimer dangling bonds by the adsorption of hydrogen, resulting in the formation of σ_{Si-H} bonds [55]. Since hydrogen is known to form pairs on the Si dimer [56], and the surface is predominantly monohydride, the change in the RAS intensity (which is additive in nature) at these energies is likely to be linearly proportional to the number of dangling bonds eliminated by hydrogen, and hence the surface hydrogen concentration. This is

supported by the observation that the integrated change in RAS signal between 1.9 and 2.9 eV yields a measurement of 'hydrogen coverage' during growth which is consistent with existing temperature programmed desorption measurements [57]. Hence, time-resolved measurements of the RAS signal at 2.7 eV (the energy below E_1 which provides the largest change in RAS intensity) have been used to provide an *in situ* monitor of surface hydrogen concentration during isothermal desorption measurements.

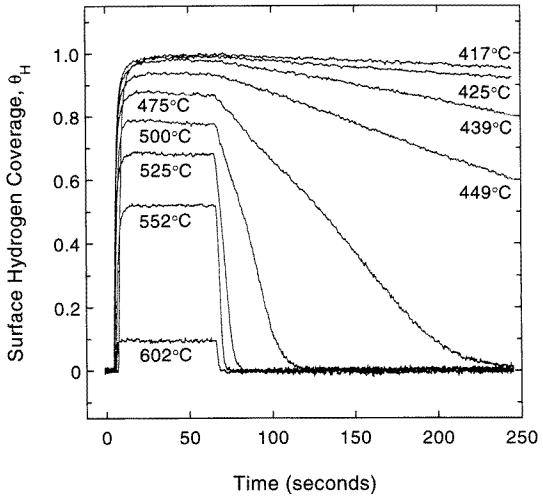

Figure 19. Isothermal measurements of hydrogen desorption from vicinal Si(001) surfaces. The coverage is scaled from changes in the RAS response at 2.7 eV (after [59]).

Figure 19 shows the surface hydrogen coverage, as determined from the RAS response, as a function of both time and temperature. The early part of each decay curve can be seen to exhibit a linear dependence of coverage with time, which changes to an exponential-like dependence as the coverage approaches zero. This observed linear dependence requires that the rate of desorption be independent of the coverage itself, i.e. it follows zeroth-order desorption kinetics. This is contrary to measurements performed on nominally *on-axis* Si(001), where hydrogen desorption was reported to be a first-order process [58].

Zeroth-order kinetics dictate that a saturated precursor state must be involved in the desorption pathway. Under these conditions, it is not the supply of atoms or molecules to this precursor state which is the rate limiting step, but rather the barrier to desorption from these states. Saturation of the precursor states can only be maintained if they are localized, existing in low and constant density. Possible candidates for precursor sites include both surface defects and surface steps. Lees *et al* have advanced an argument in favour of precursor sites which are associated with surface steps [59]. According to this model, the growth rate of an epitaxial layer should be dependent on the extent of misorientation, in the temperature regime where there is a saturated hydrogen coverage. To test this hypothesis, Si layers have been grown on two substrates with different misorientations, at $\sim$500 °C. The thickness of the layer grown on the 4° misoriented surface was found to be 20% greater in comparison to the nominally singular surface [60], thus confirming that a greater step density leads to a greater localized desorption site density, and consequently a higher desorption and growth rate.

It is important to note that the existence of a step- (or defect-) mediated desorption pathway does not preclude desorption from the terraces. At low temperatures, the difference in desorption rate between surfaces with different step density (different misorientation) is quite large, with the higher step density giving rise to a larger rate. At higher temperatures, the differences become smaller as desorption from the terraces increases its contribution to the overall desorption process. The balance between the two is then governed by the temperature, the density of precursor sites and the activation barriers for the two different desorption pathways. This is reflected in a small misorientation dependence of the rate constant. Introduction of Ge also modifies the balance between the two possible desorption pathways as the Ge–H bond is expected to be weaker compared to the Si–H bond. In this case, isothermal measurements of hydrogen coverage from SiGe surfaces exhibit a purely exponential time dependence, consistent with desorption dominated by terrace sites [61].

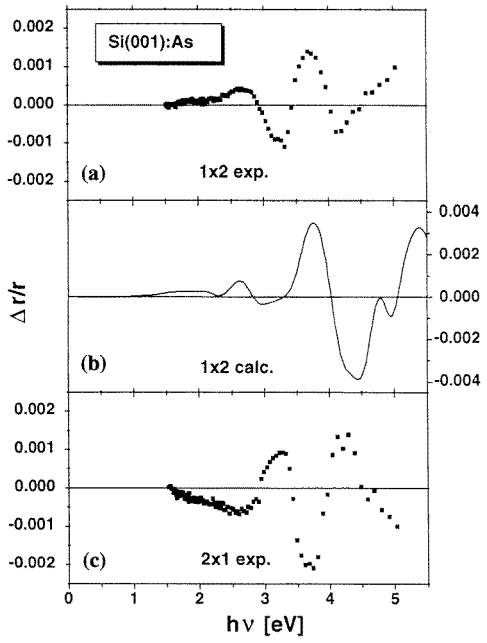

Figure 20. (a) RAS spectrum of the vicinal Si(001):As–(1 × 2) surface, (b) calculation for the Si(001):As–(1 × 2) reconstruction, (c) RAS spectrum of the orthogonal Si(001):As–(2 × 1) reconstruction, prepared by dosing the surface with As_4 at 500 °C (after [21]).

5.5. Studies of adsorption on Si(001)

Kipp *et al* have used a combination of RAS and STM measurements carried out *in situ*, at room temperature, to study As-terminated Si(001) surfaces [21]. The STM images reveal that saturating the clean Si(001)–(2 × 1) surface at room temperature in an As_4 flux, and then ramping the sample to 600 °C before turning the As flux off, produces a Si(001):As–(1 × 2) surface. Figure 20(a) shows the RAS spectrum obtained from a surface prepared in this manner, whilst figure 20(b) depicts the corresponding calculated RAS response. It can be seen that there is excellent agreement. Figure 20(c) shows the RAS spectrum obtained from a clean Si(001)–(2 × 1) surface dosed with As_4 at 500 °C to produce the Si(001):As–(2 × 1) reconstruction. It can be seen that this surface dimer orientation gives rise to a change

in sign of the principal features in the RAS spectrum, in this case at energies of 3.7 and 4.3 eV. The cases of Si(001):As–(2×1) and Si(001):As–(1×2) correspond to the As–As dimers running parallel or perpendicular to the step edges.

Whilst it is tempting to conclude that the RAS response from Si(001) surfaces mirrors that shown by GaAs(001) surfaces, this is not the case. It has been shown in experiments on Ga and As adsorption on the GaAs(001) surface [9] that the sign of the RAS signal depends mainly on the dimer orientation, rather than the particular nature of the adsorbed atomic species. However, Power *et al* [62] have found recently that the RAS spectra from Ga and Sb adsorbed on the Si(001)–(1×2) surface differ in sign, even though the surface dimers are aligned in the same direction!

6. Monitoring growth and surface morphology

It is well known, from RHEED intensity oscillations during MBE growth, that in a layer-by-layer growth mode the surface morphology oscillates between the extremes of being smooth and half-covered with monolayer islands. Since the early days of the technique RAS has also been capable of detecting such monolayer oscillations although their origin appears to be more complex than in the case of RHEED, as will become apparent. In this section growth oscillations on a variety of substrates are discussed in addition to the low-temperature overgrowth of Si/GaAs(001) structures in which surface disorder plays a role.

6.1. Growth oscillations for GaAs-based materials

Figure 21(a) shows the RAS response, monitored at an energy of 2.6 eV, for the growth of an $In_{0.11}Ga_{0.89}As$ (5 ML)/GaAs (10 ML) superlattice with 30 periods [17]. It can be seen that the (composition-related) 30 individual periods appear nearly identical, which suggests that all the periods of the superlattice are equal. In addition, the 'envelope' of the RAS signal arises from two periods of the optical Fabry–Pérot-like interference, which occurs between the GaAs buffer layer and the sample surface. Figure 21(b) contains an expanded view of the RAS signal during the growth of one superlattice period, where the monolayer oscillations are both clearly present and easily distinguishable [17]. In this case these were attributed to oscillations in dimer configuration occurring for domains close to surface steps.

Ploska *et al* [11] have carried out a comparison between growth oscillations obtained for GaAs under MBE and MOVPE conditions. Their results serve to confirm that a necessary condition for the appearance of RAS oscillations, for both growth techniques, is the formation of islands which result in a maximum surface roughness at half-monolayer coverage. For MBE, the RAS oscillations can be modelled using an effective medium approach [6] on the basis that the islands, as well as the area in between the islands, is (2×4) reconstructed. However, the RAS oscillations observed in MOVPE growth reveal a distinct difference in phase when compared with the MBE growth oscillations [11]. This disparity has led Ploska *et al* to deduce that the origin of RAS oscillations in MOVPE is more complex, with the growing surface containing an oscillating mixture of $c(4 \times 4)$ and (1×6)-like surfaces.

6.2. Growth oscillations for InP

As noted earlier in section 2, the RAS spectrum for the static InP(001) surface, under the standard conditions of temperature and pressure used for InP growth by MBE, corresponds

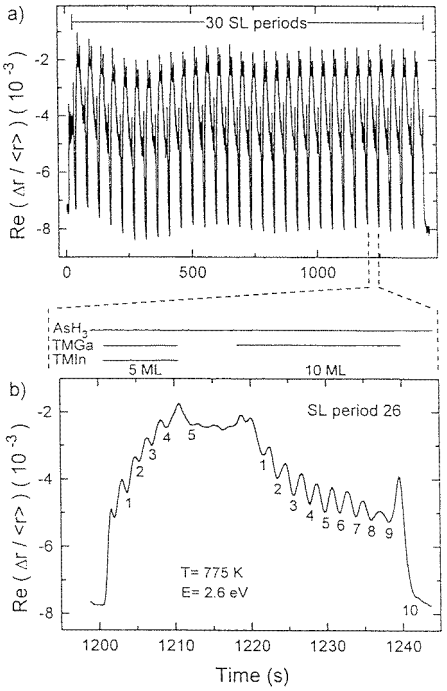

Figure 21. (a) RAS response for the growth of an InGaAs (5 ML)/GaAs (10 ML) superlattice with 30 periods. (b) Magnification of the RAS response for the growth of one period of the superlattice (after [17]).

to that of the $(2 \times 4)\beta$ surface reconstruction. Experiments [14, 15] show that on initiating growth there is a change in the RAS signal, attributable to a decrease of phosphorus coverage at the surface, which is consistent with the stable surface reconstruction becoming $(2 \times 4)\alpha$. During subsequent growth, the monolayer oscillations in RAS intensity possibly reflect variations in the surface P coverage in a manner analogous to that previously observed for GaAs surfaces. Detailed experiments, at a photon energy of 2.0 eV, have shown that relatively small changes in either temperature, or phosphorus beam equivalent pressure, can have a dramatic effect on the quality of the observed oscillations. Figure 22 shows oscillations in RAS intensity during InP growth by MBE, at a growth rate of 0.34 ML s^{-1}, for substrate temperatures between 450 and 490 °C. In each case, there is 30 s of growth followed by 10 s where the In shutter is closed, then another 10 s of growth. It can be seen there is a narrow range of temperature, centred around 470 °C, for which the oscillations in RAS intensity are most clearly defined. This 'optimal' temperature decreases systematically with decreasing phosphorus flux, and also shows a weak variation with the growth rate itself.

6.3. Growth oscillations for Si

In section 5.3 we discussed the use of vicinal Si(001) substrates when studying desorption of hydrogen from Si surfaces, in order to minimize variations in domain coverage. Growth studies, performed with *on-axis* Si(001) substrates, have revealed periodic oscillations in both RHEED specular beam and RAS intensities [55]. Whilst the RHEED oscillations exactly follow the periodic variations in surface step density associated with monolayer

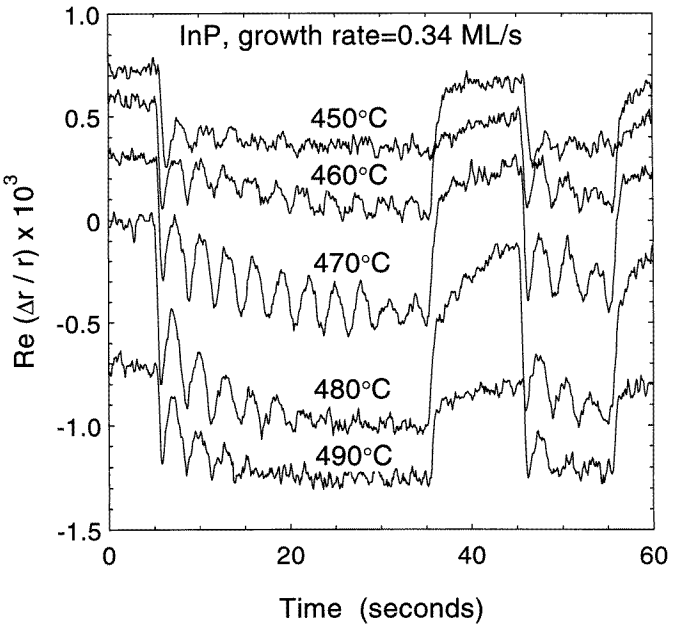

Figure 22. Time-resolved RAS measurements, monitored at an energy of 2.7 eV, for InP growth on InP(001) by MBE using elemental sources.

growth, the RAS signal oscillates with double this periodicity. Figure 23, taken from Zhang *et al* [55], is a schematic diagram which illustrates the variations in both domain coverage and RHEED intensity during growth. The left-hand column depicts the state of the Si(001) surface during Si deposition, with the symbols α and β being used to label the (2×1) and (1×2) domains, respectively. The starting surface is assumed to be dominated by one domain, α, and growth is assumed to be monolayer-by-monolayer occurring by 2D nucleation, 2D island growth and step annihilation via coalescence of 2D islands. The middle column shows the familiar response of the RHEED specular beam intensity to layer-by-layer growth, while the right-hand column illustrates the changes in relative domain coverage, $\Delta\theta = \theta_\alpha - \theta_\beta$, where θ_α and θ_β are the coverages of the α and β domains. Since the RHEED signal is very sensitive to the step density, its intensity changes from a maximum through a minimum and returns to a maximum, thus completing one oscillation for the deposition of a monolayer. During the same period, the domain coverage changes from dominance by type α to dominance by type β, and hence explains why the RAS signal oscillates with double the period of the RHEED intensity.

Figure 24 contains oscillations in RHEED and RAS intensities obtained during growth of Si at a temperature of 600 °C, a near-optimal temperature at which to observe RAS oscillations. In fact, the temperature range for which oscillations in RAS intensity can be discerned lies between 550 and 650 °C. In comparison, RHEED oscillations can be observed at all temperatures below 650 °C. This high-temperature limit arises from a change in growth mode to step flow, with a resulting lack of variation in step density. The low-temperature limit for RAS oscillations, of 550 °C, reflects the fact that the surface becomes increasingly covered with hydrogen at these temperatures as discussed in section 5.3 [55].

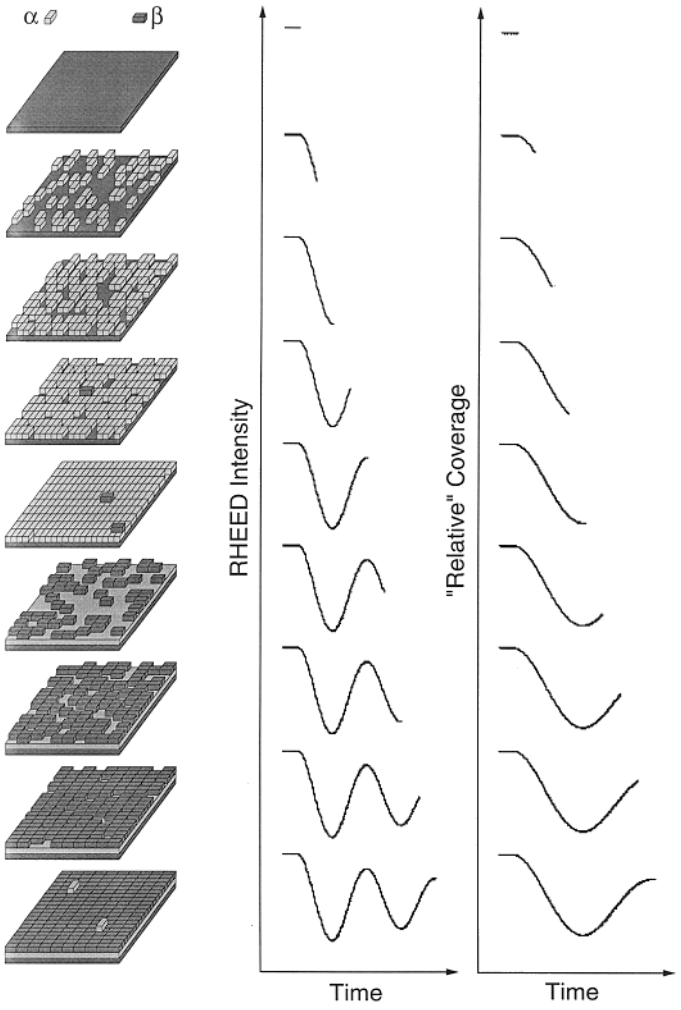

Figure 23. Schematic representation of the Si surface during growth, showing the expected variations in RHEED intensity and surface domain coverage (after [55]).

6.4. Monitoring low-temperature GaAs overgrowth of Si/GaAs(001)

In section 4.1 and 4.2 we discussed the use of RAS to study the deposition of sub-monolayer coverages of Si and Be, on the GaAs(001) surface, for applications relating to δ-doping. The reason for restricting all measurements to deposition temperatures of 400 °C was simply that this temperature affords the best compromise in terms of the electrical quality of the material, and the confinement of the dopant atoms to the delta plane. In our investigation of the overgrowth of GaAs on Si/GaAs(001), both the Si and subsequent GaAs depositions have been carried out at substrate temperatures of 400 °C. Hence, we initially sought to ascertain the similarity between GaAs surfaces grown at 400 °C and those grown at 580 °C, then cooled to 400 °C [63]. Our results indicate that growth at lower substrate temperatures (e.g. 400 °C) results in a disordered surface that, when growth is terminated, slowly recovers to a well ordered surface once more.

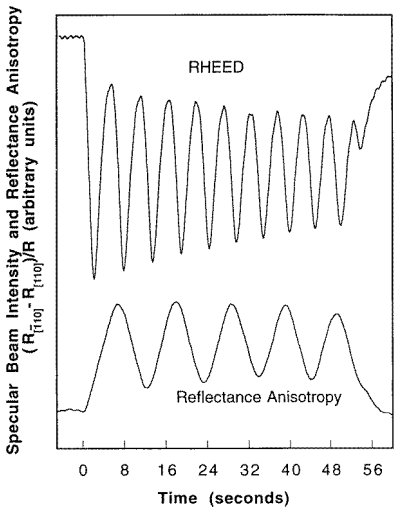

Figure 24. Comparison between RHEED and RAS oscillations obtained during Si growth on the Si(001) surface at 600 °C (after [55]).

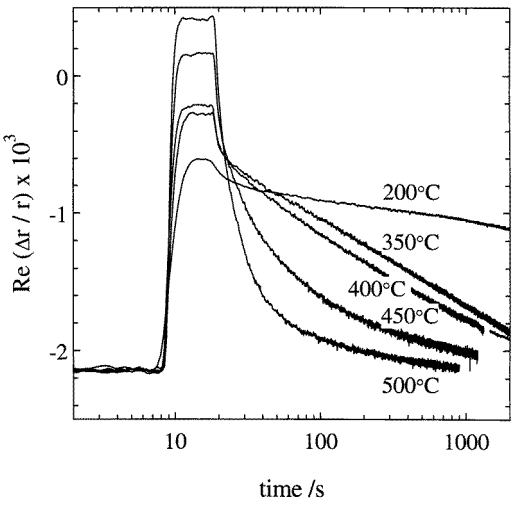

Figure 25. Time-resolved RAS measurements, monitored at an energy of 2.65 eV, for 10 s growth of GaAs at the substrate temperatures indicated.

Figure 25 contains time-resolved RAS measurements, obtained at an energy of 2.65 eV, for 10 s GaAs growth at substrate temperatures from 200 to 500 °C. Each curve has been aligned so as to give the same signal level prior to the onset of growth. The initial equilibrium signal, the different equilibrium reached during the 10 s growth, and the return towards the initial equilibrium following growth are evident. These changes correlate with observations of the RHEED pattern during this procedure, where the original very sharp c(4 × 4) reconstruction is quickly replaced on growth with a disordered (1 × 1)-like pattern which only very slowly recovers to a good c(4 × 4) after growth has been terminated. As noted previously [63], a timescale of >1 h is required to recover the intensity of the

2.65 eV minimum at a growth temperature of 400 °C. This is an unrealistically long time to use when studying GaAs overgrowth on Si/GaAs by a cycle of sequential growth and RAS measurements. Hence, we chose to record systematically RAS spectra 5 min (300 s) after each deposition. Since each RAS spectrum is acquired in ∼3 min (180 s), this means that the intensity of the 2.65 eV minimum changes by ∼7.5% during each scan.

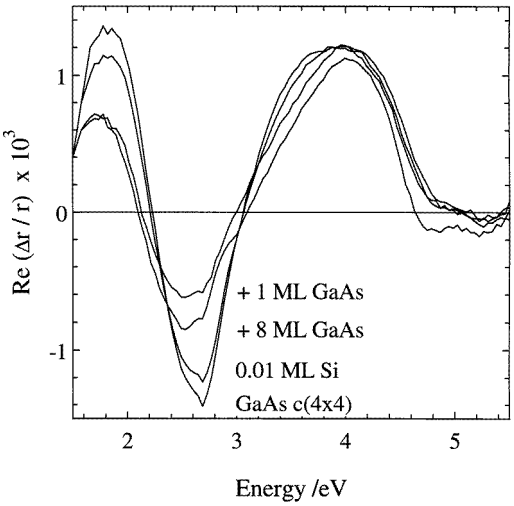

Figure 26. RAS spectra at 400 °C for the initial GaAs(001)–c(4 × 4) surface, following addition of 0.01 ML Si and the first stages of overgrowth with GaAs (after [63]).

Figure 26 shows a series of RAS spectra that correspond to the initially clean GaAs(001)–c(4 × 4) surface, its modification with the addition of 0.01 ML Si and the first stages of overgrowth with GaAs. The RAS spectra for GaAs overlayer thicknesses of 2 and 4 ML have been omitted for clarity. Most noticeably, deposition of 0.01 ML Si is seen to give rise to an upward shift of the 2.65 eV minimum, which becomes enhanced greatly on overgrowth with 1 ML GaAs. Increasing GaAs coverage systematically reverses the shift obtained for 1 ML GaAs (the omitted RAS spectra for depositions of 2 and 4 ML lie between those shown for 1 and 8 ML). While it is tempting to attribute the shift of the 2.65 eV minimum solely to a growth-temperature-induced decrease in surface order, and this does appear to be the main contributing factor, it also seems likely that disorder induced by overgrowing the Si δ-layer is also present. In addition, contributions from the linear electro-optic effect must also be considered and these will be dealt with in detail in the following section.

7. Interpreting RAS spectra from doped semiconductor structures

When RAS measurements are performed on doped semiconductor substrates, there is a contribution to the RAS lineshape which arises from the electric field within the surface depletion layer. The dependence of RAS response on the electric field at the surface of a semiconductor has been studied previously for uniformly bulk-doped GaAs [64, 65] and has been shown to give rise to a feature in the RAS spectrum at around 3 eV. This feature has been attributed, in turn, to the linear electro-optic (LEO) effect, associated with the E_1 and $E_1 + \Delta_1$ interband transitions. However, it has never been clearly demonstrated to what

extent this is a surface (e.g. arising from the interaction of the surface electric fields with surface states) or a bulk effect.

7.1. RAS spectra from δ-doped GaAs(001)

The application of δ-doping, to studying the effect of doping on RAS spectra, has advantages over coventional bulk doping since it makes it possible to alter the strength of the depletion electric field in two ways: either by changing the *concentration* of Si atoms in the δ-layer, or by varying the *position* of the δ-layer with respect to the sample surface. Thus, it becomes possible to examine, in a much more controlled manner, the influence on RAS of the depletion electric field. In addition, as the concentration in the δ-layer is increased it is well established that the dopant starts to become inactive at relatively modest ($\sim 10^{13}$ cm^{-2}) levels. Since only active dopants make a contribution to the electric field the level of activity may also be monitored using this technique, a task that has proved difficult by other techniques.

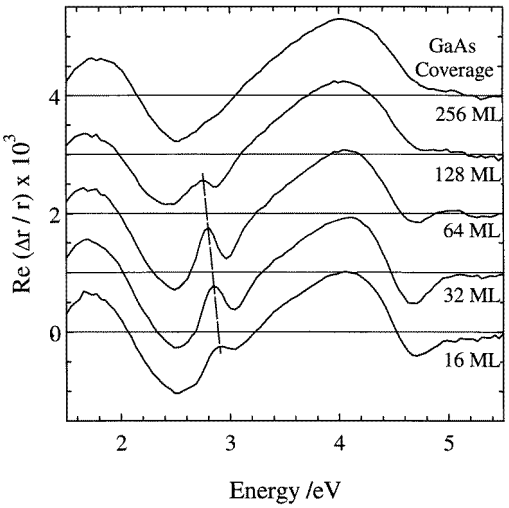

Figure 27. RAS spectra for increasing GaAs coverage on top of 0.01 ML Si/GaAs, showing the development of the LEO feature at ∼2.9 eV. The dashed line follows the redshift (after [63]).

Figure 27 shows a series of RAS spectra obtained following overgrowth with 16, 32, 64, 128 and 256 ML GaAs on top of 0.01 ML Si/GaAs(001). Each spectrum is plotted using the same absolute scale, but displaced vertically for clarity. The position of the zero line has been included in each case. The RAS spectrum for 16 ML GaAs shows an inflection at ∼2.9 eV, the signature of an LEO-related feature. The intensity of the LEO feature is found to increase initially with GaAs coverage, reach a maximum at an overlayer thickness of 64 ML GaAs and then decrease with additional GaAs coverage. At the same time, there is a corresponding redshift (maximum value ∼100 meV) in energy of the LEO feature (as indicated by the dashed line in figure 27). One might expect the decrease in LEO intensity for thicknesses >64 ML GaAs to be explicable simply by the electric field at the surface decreasing as the δ-layer is buried more deeply, or the δ-layer moving beyond the penetration depth of the light, but this does not explain the behaviour for thicknesses less than 64 ML.

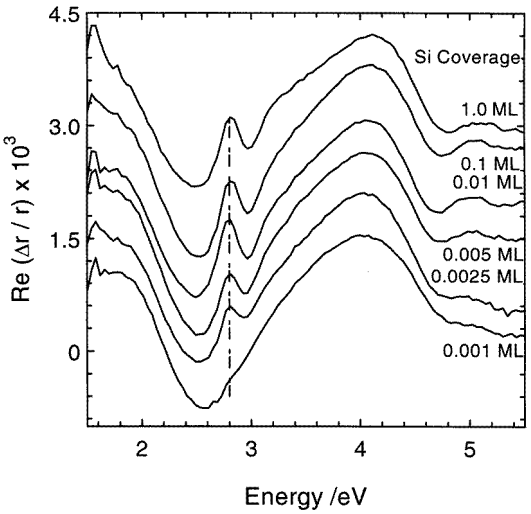

Figure 28. RAS spectra for 64 ML GaAs deposited on Si/GaAs, where the Si coverages vary from 0.001 to 1.0 ML (after [63]).

In figure 28 we display RAS spectra for overgrowth with 64 ML GaAs, the thickness at which the LEO feature is fully developed, on all the Si sub-monolayer coverages we have studied. Once again, all spectra have been plotted with the same absolute scale, but displaced vertically for clarity. The overall shapes of the RAS spectra are remarkably similar, excluding the contribution of the LEO-related feature, considering that the Si coverages span three orders of magnitude from 0.001 to 1.0 ML. It is to be noted, from our previous RAS measurements for Si on GaAs(001) [31], that an Si coverage of 0.1 ML corresponds to a crossover in the behaviour of the 2.65 eV feature. At coverages of <0.1 ML Si, both c(4×4) and (2×1) reconstructions appear to co-exist and so the overall RAS signal contains contributions from both surface phases. It is evident that the intensity of the LEO-related feature increases with Si sub-monolayer coverage up to 0.01 ML, and then decreases slightly with further coverage up to 1.0 ML Si. A similar correspondence has been reported between the density of Si_{Ga} (i.e. Si on donor sites) and the total Si coverage, up to a coverage of $\sim 10^{13}$ cm^{-2} (0.016 ML) [66]. In that case, the measured density of Si_{Ga} then remained approximately constant up to a coverage of $\sim 4 \times 10^{14}$ cm^{-2} before beginning to decrease, in good agreement with the results presented here. Figure 28 also indicates that, in this case, there is no observable variation in energy of the LEO feature with Si sub-monolayer coverage.

7.2. Comparison of calculated surface and near-surface fields with LEO intensity

For uniform doping, to a good approximation the electric field in the surface depletion region of the GaAs is a maximum at the surface of the sample and decreases linearly with distance into the sample, reaching zero at the depletion width. Introducing a δ-layer produces a more complex behaviour: to a rough approximation (if the δ-layer is not too far from the surface compared with the depletion width) the electric field is constant from the surface to the δ-layer, and then decreases linearly with distance beyond the δ-layer (reaching zero at a distance less than the depletion width without δ-doping). For our samples, this behaviour happens on a length scale comparable to the penetration depth [67] of the incident radiation

at 3 eV (∼17 nm or 60 ML GaAs). The influence of the electric field, normal to the sample surface, on the RAS feature is known to be linear in field amplitude [64]. The data of figure 27 cannot be interpreted using the electric field exactly at the surface, however, since this decreases monotonically with depth of the δ-layer. We therefore define the quantity

$$\langle E\rangle = \frac{\int_0^L \mathrm{e}^{-x/\lambda}E(x)\,\mathrm{d}x}{\int_0^L \mathrm{e}^{-x/\lambda}\,\mathrm{d}x} = \frac{1}{\lambda(1-\mathrm{e}^{-x/L})}\int_0^L \mathrm{e}^{-x/\lambda}E(x)\,\mathrm{d}x \to \frac{1}{\lambda}\int_0^\infty \mathrm{e}^{-x/\lambda}E(x)\,\mathrm{d}x$$

which reflects the *average* field as experienced by the light. We shall refer to this last integral as the *integrated surface field*. Here λ in these calculations is the experimentally determined penetration depth of 17 nm, for GaAs at a photon energy of 3 eV [65].

For uniform (bulk) doping, it is easy to obtain an analytic expression for the field from the surface into the bulk and hence evaluate the integrated surface field. With non-uniform (δ-) doping, however, we need to find the exact solution of Poisson's equation in the near-surface region numerically. This was done by solving self-consistently the finite-difference representation of Poisson's equation using a straightforward shooting method.

In the calculation [68], the incorporated Si atoms are assumed to form an ideal uniform delta sheet of donors (i.e. all electrically active and not spread in the x-direction) within the GaAs crystal. Background bulk doping levels of 2×10^{15} cm^{-3} (n-type, donor ionisation energy 0.0053 eV) and 1×10^{15} cm^{-3} (p-type, acceptor ionization energy 0.020 eV) were assumed. Electron and hole effective masses were taken as 0.067 and 0.41 times the free electron mass, respectively. The GaAs bandgap was taken as 1.42 eV, and the relative permittivity as 13.1. The surface barrier was taken as 0.72 eV. One monolayer of GaAs is taken to have a thickness of 0.2825 nm. For the Si doping, a surface concentration of one monolayer is equivalent to 6.265×10^{14} atoms cm^{-2}.

In previous studies [64, 65], an accurate determination of the integrated LEO area was facilitated by being able to subtract the RAS spectrum for an undoped GaAs(001) sample from the spectra obtained for GaAs layers with different degrees of bulk doping, but similar surface structure. In the present case (as discussed earlier), the RAS spectra for GaAs overgrowth on 0.01 ML Si/GaAs are not identical to that for the clean GaAs(001)–c(4×4) surface, hence the integrated LEO area cannot be obtained by a similar process of spectral subtraction. The approach taken here has been to interpolate linearly between two points on either side of the LEO feature, and to integrate numerically the deviation of the RAS data over this region.

Figure 29 contains a comparison between the calculated surface field and integrated surface field values for GaAs overgrowth on 0.01 ML Si/GaAs. The superimposed experimental data have been multiplied by a scale factor to facilitate comparison with both calculated curves. It is evident that the observed decrease in LEO intensity for overlayer thicknesses both above and below 64 ML GaAs is reproduced extremely well by the behaviour of the integrated surface field. The maximum in integrated surface field can be understood qualitatively as follows. The electric field between the surface and the δ-layer can be fairly high compared with the ordinary depletion field (particularly when the layer is close to the surface and heavily doped), and so will contribute strongly to the integral for the integrated surface field. However, the *range* of its contribution to the integral is small (zero, in the limit that the δ-layer is *at* the surface) and increases as it moves further from the surface. As the δ-layer moves still further from the surface, however, the reduced field between the δ-layer and the surface decreases its contribution to the integral. In addition, consideration of the fact that the δ-layer moves through the penetration depth of the incident radiation also explains the redshift of the LEO feature with increasing GaAs thickness seen in figure 27 [69].

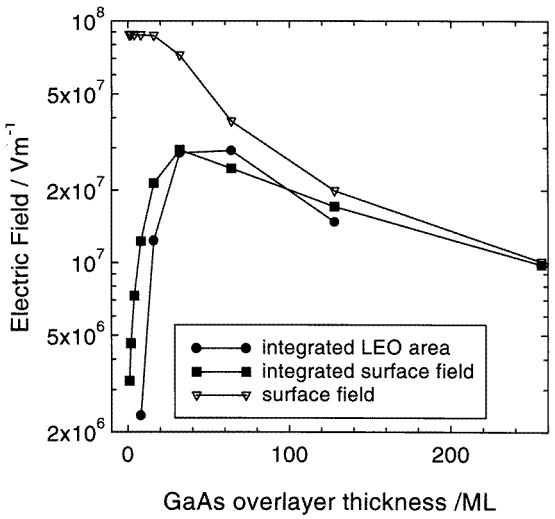

Figure 29. Calculated values of surface and integrated surface fields for GaAs overgrowth on 0.01 ML Si/GaAs, together with experimentally determined LEO intensities.

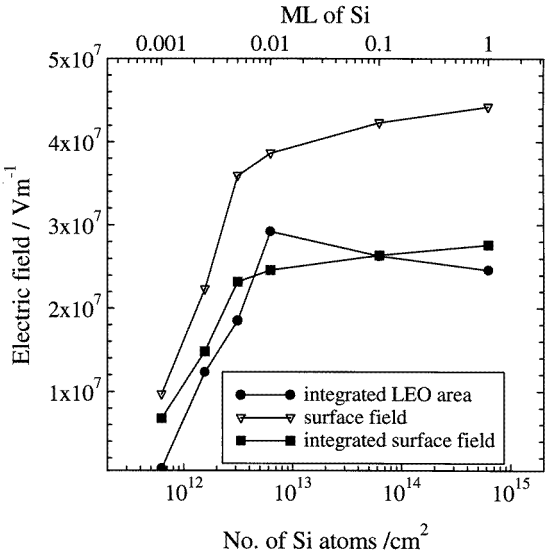

Figure 30. Calculated values of surface and integrated surface fields for 64 ML GaAs overgrowth on Si/GaAs, and comparison with measured LEO intensities, where the Si content ranges from 0.001 to 1.0 ML (6.27×10^{11} to 6.27×10^{14} atoms cm^{-2}).

Figure 30 shows a similar comparison between the calculated surface field and integrated surface field for 64 ML GaAs overgrowth on all the Si sub-monolayer coverages we have studied. Once again, the LEO intensities have been multiplied by a scale factor, *identical* to that used in figure 29. In this case, there is little to choose between the two calculated dependencies of field on Si content, since both curves follow the slope of the experimental data for low Si concentrations before reaching a knee around 6×10^{12} atoms cm^{-2} (0.01 ML

Si). From this point, the calculated curves continue to show an increase with Si content, whilst the LEO intensity decreases. Such a disparity is to be expected, however, since the solution of Poisson's equation in these cases assumes all the Si atoms to be electrically active, i.e. does not allow for the saturation in the number of Si donors which is known to occur [66] and is apparent in the integrated LEO area data.

8. Strain relaxation and self-ordering

RAS measurements can be used to determine the strain present in overlayers which have been grown pseudomorphically on top of a different substrate material, since the RAS signal from the strained surface dimer species will be shifted in energy from its value on a relaxed surface. In practice, these energy shifts are often actually quite small (but nevertheless detectable) compared with the width of the RAS features, unless the system studied is highly mismatched in terms of lattice parameter. InAs/InP provides an example of such a system, where there is a sufficient mismatch in lattice constants (3.1%) to result in a significant difference between RAS spectra obtained from thin pseudomorphic InAs/InP layers and bulk InAs. At the same time, the mismatch is small enough so that strain relaxation only starts to occur for InAs thicknesses greater than 5 ML [39]. In the section which follows, we shall proceed to describe RAS measurements from a more highly mismatched system, InAs on GaAs.

8.1. Growth of InAs on GaAs(001)

It is well known that as films of InAs are grown on GaAs(001) they undergo a number of structural transitions as their thickness is increased [70]. Initially, the InAs is pseudomorphically strained to the GaAs substrate but, due to the large mismatch in lattice constants ($\sim$7.2%), InAs islands such that it is commensurate with the substrate for thicknesses in excess of $\sim$1.6 ML. With increased thickness misfit dislocations are generated and the islands coalesce to form a continuous but relaxed film. Whilst such *self-organized* behaviour has obvious potential for the formation of arrays of quantum dots, the main stumbling block to application in practical devices has been island uniformity. RAS, with its high degree of surface sensitivity, provides an excellent *in situ* technique with which to study the factors which control the islanding process in *real time*.

Figure 31 contains RAS spectra obtained from a clean GaAs(001) surface at 350 °C, and following deposition of 0.2 and 1.6 ML InAs. Both the amplitude and the sign of the '2.7 eV' signal are found to change (and it shifts to lower energy) as the deposited InAs thickness is increased to 1.6 ML, whilst there is only a change in amplitude of the signal at 4.0 eV. Upon initiation of InAs growth, RHEED observations showed an initial gradual change from a c(4×4) pattern to an 'asymmetric' (1×3) pattern at $\sim$0.3 ML InAs coverage, where the 3× features were slightly offset towards the half-order position. With increasing coverage up to 0.7 ML the 3× features developed, moving towards their correct positions, i.e. the (1 × 3) pattern became 'symmetric'. Above 1 ML the pattern gradually changed to (1 × 1) before becoming spotty, indicative of islanding at $\sim$1.6 ML; post-growth, the RHEED spots slowly sharpened with time.

In order to follow the dynamics of the system, including the possible influences of In re-evaporation and redistribution on the surface following islanding, time resolved RAS measurements were performed at 2.6 eV and 4.0 eV, for the deposition of 2 ML of InAs at a growth rate of 0.025 ML s^{-1}. The RAS data contained in figure 32 and obtained for a growth temperature of 450 °C display the characteristic features of virtually all such time-resolved

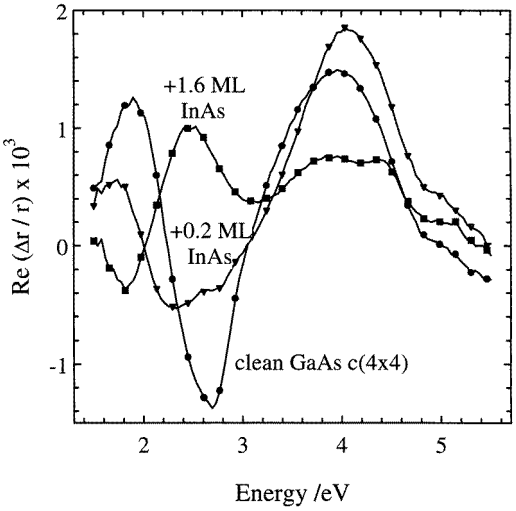

Figure 31. RAS spectra measured at 350 °C, for the clean GaAs(001)–c(4 × 4) surface, and following deposition of 0.2 and 1.6 ML InAs.

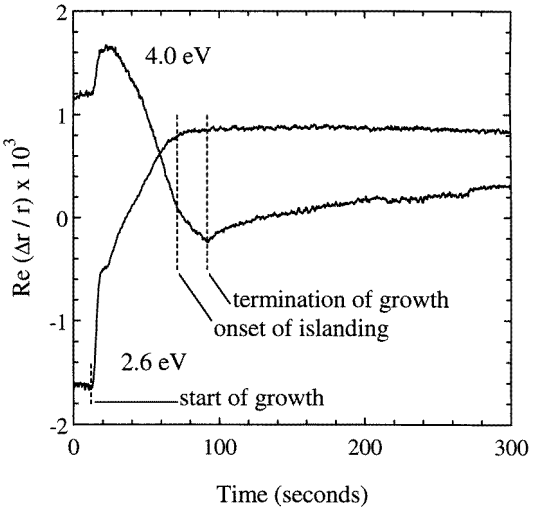

Figure 32. Time-resolved RAS measurements, obtained at energies of 2.6 and 4.0 eV, during the deposition of 2 ML of InAs onto GaAs(001), at a growth rate of 0.025 ML s^{-1} and a substrate temperature of 450 °C.

measurements under different conditions and may be compared with the spectroscopic changes apparent in figure 31. Upon initiation of growth, both the 2.6 and 4.0 eV RAS signals increase very rapidly before briefly saturating at ∼6 to 12 s corresponding to 0.15 to 0.3 ML and to the loss of the c(4 × 4) pattern. The 2.6 eV response then returns to a (less steeply) rising signal once more, whilst the 4.0 eV intensity decreases towards zero. At the onset of islanding (∼1.6 ML), the 2.6 eV signal is seen to saturate, as has been observed previously [58–60], but, by contrast, at 4.0 eV there is no dramatic discontinuity although there is a slight reduction in the slope. Remarkably, there is absolutely no indication of

the cessation of growth or of any significant post growth changes at 2.6 eV, whilst both a strong discontinuity at cessation of growth and significant post growth changes are observed at 4.0 eV. The main points to note are therefore:

(i) the sensitivity of the 2.6 eV signal and lack of sensitivity of the 4.0 eV signal to the onset of islanding,

(ii) the total absence of any indication of the cessation of growth at 2.6 eV concurrent with a very strong discontinuity at 4.0 eV,

(iii) the sensitivity to post-growth surface changes at 4.0 eV only.

Although detailed calculations will be necessary to understand these effects properly [26] it is possible to consider the onset of islanding, cessation of growth and post-growth development on a phenomenological basis. In general, the RAS signal in such a system as this will include contributions from the surface order, the thickness of the overlayer and possibly also the nature of the buried interface [72–74]. Since the islands formed initially are small and cover a small fraction of the surface [75] they are unlikely to contribute significantly to the RAS signal. Therefore, ignoring any possible interface effects, the constant signal at 2.6 eV following islanding may result either from:

(a) a balance between the effects of a changing surface order and an increasing inter-island film thickness,

(b) a constant (in both surface order and thickness) inter-island film,

(c) a constant surface contribution and a negligible effect from an increasing inter-island film thickness.

Although none of the above possible explanations can be definitely ruled out (b) requires that all of the incident In flux is directly transferred to the islands and is contradicted by the observation that the 4.0 eV signal is relatively unaffected by islanding. Both (a) and (c) indicate that the thickness of the inter-island film continues to increase beyond the point of islanding and, in particular, (c) implies that there might be a simple relationship between the continuing changes in the 4.0 eV signal and the inter-island film thickness.

The prediction of an anomalously thick unstable inter-island film leads to the expectation of subsequent redistribution of material to the islands through a kinetically limited process which may be monitored by observation of the 4.0 eV time-resolved signal. It also suggests a test for this interpretation, i.e. that increasing/decreasing the growth temperature should increase/decrease the rate of distribution respectively. Figure 33 shows time-resolved scans, acquired at a photon energy of 4.0 eV, for the deposition of 2 ML of InAs at a growth rate of 0.025 ML s^{-1}, for temperatures of 350, 475 and 500 °C. Differences at the onset of growth relate to the initial reconstruction changes (c(4 × 4) or (2 × 4) to (1 × 3)) which took place more quickly with increasing growth temperatures. However, it is the point of islanding and following the cessation of growth that are of most interest here. At 350 °C there is only the slightest inflection at the point of islanding and consequently the RAS signal decrease can be seen to be virtually in proportion to the deposited thickness for InAs thicknesses greater than ∼0.8 ML and up to at least 2 ML. Thus it appears that in this range the 4.0 eV RAS response provides a direct measure of the inter-island thickness and that even beyond the point of islanding most of the incident In flux continues to be incorporated into the continuous inter-island film at this growth temperature. In contrast at higher temperatures, although the response varies linearly from 0.8 ML up to the point of islanding, here its inflection becomes more pronounced so that at 500 °C and above a flat trace is obtained until cessation of growth, implying that under these conditions all of the incident flux is incorporated immediately into islands. All of these observations are

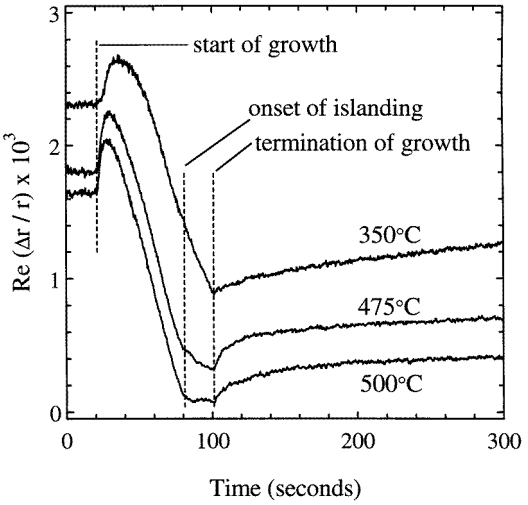

Figure 33. Time-resolved RAS measurements, obtained at an energy of 4.0 eV, during deposition of 2 ML of InAs onto GaAs(001), at a growth rate of 0.025 ML s^{-1}, and substrate temperatures of 350, 475 and 500 °C.

consistent with the model put forward in this section, and serve to confirm that the RAS signal at 4.0 eV provides a useful tool for *real time* monitoring of the redistribution of InAs on GaAs(001).

8.2. Simulating the RAS data for growth of 2 ML InAs on GaAs(001)

The following model is a simple simulation of the thickness of the 'InAs' wetting layer through the deposition and post-growth rearrangement processes. It is not intended to be an accurate representation of the physical processes which occur, but it does serve to illustrate some of the issues that a more realistic model should address. Whilst the model does provide a reasonable agreement with the RAS data, it should be remembered that any comparisons are made on the assumption that the 4.0 eV RAS data does indeed reflect the wetting layer thickness above InAs coverages of ∼0.8 ML.

Changes in the wetting layer thickness (WL) come from growth, which arises from the incident In and As_4 fluxes, as well as loss of material to islands which are considered as effectively invisible to the RAS measurement at this photon energy. The growth rate (g_r) used is the same as the experimental value of 0.025 ML s^{-1}, which for 2 ML deposition corresponds to a growth time of 80 s. The change in wetting layer thickness in 1 s (δ(WL)) is thus given by:

$$\delta(\mathrm{WL}) = g_r(1 - f) - A\,\mathrm{sink}\,(\mathrm{WL} - 1.6) - B(\mathrm{WL} - 1)$$

where all thicknesses are expressed in monolayers.

In the first term, f is the fraction of incident flux removed from the wetting layer when the thickness of the wetting layer is greater than 1.6 ML, the critical thickness for islanding (i.e. f is 0 for WL < 1.6 ML, and so non-zero values for f only occur during the islanding process). An alternative approach would be to remove material proportional to the excess thickness over 1.6 ML. The reason for employing the fractional term, f, is simply because it provides better agreement with the experimentally observed features, i.e. it provides a

clear inflection at the onset of islanding, followed by a roughly linear change in signal after this point. The second term provides the mechanism for the relatively rapid recovery of the RAS signal following cessation of growth. The quantity 'sink' represents the total amount of material transferred to islands, i.e. total deposited thickness = sink + WL (in the absence of re-evaporation). Its inclusion provides a mechanism for the efficient removal of material from the wetting layer by the islands and is included in order to successfully model the RAS data obtained with thicker islanded InAs films [76]. The (WL − 1.6) factor is prompted by the behaviour of the post-growth recovery in RAS signal, which seems to proceed rapidly back to a level characteristic of 1.6 ML InAs, and thereafter more slowly, for WL < 1.6 it becomes zero. The final term is included to account for the much slower thinning of the InAs wetting layer for thicknesses less than 1.6 ML, and is in accord with earlier spectroscopic RAS data which pointed to final equilibrium WL thicknesses of ∼1 ML [71]. A and B are scaling factors.

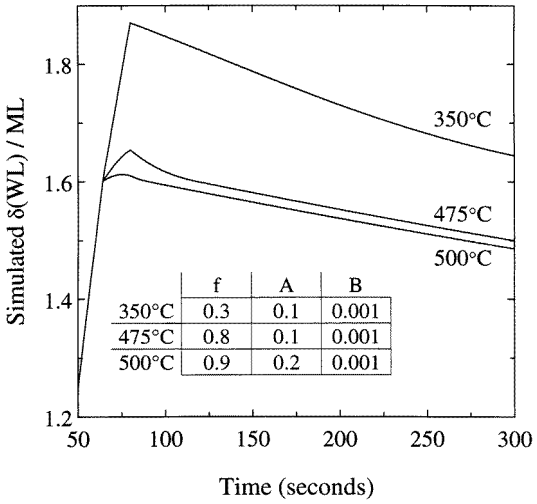

Figure 34. Simulation of the change in wetting layer thickness, δ(WL), using $\delta(\mathrm{WL}) = g_r(1-f) - A\,\mathrm{sink}\,(\mathrm{WL}-1.6) - B(\mathrm{WL}-1)$ where $g_r = 0.025$ ML s^{-1} and the values of f, A and B are as indicated in the figure.

Figure 34 contains simulations of the RAS data taken at temperatures of 350, 475 and 500 °C. The inset to this figure shows the values for f, A and B used in each case. Whilst these simulations are not meant to be best fits to the experimental data they do, to a first approximation, mimic the results obtained from the variable-temperature study of 2 ML InAs deposition on GaAs(001). It can be seen that the values for both f and A increase with $T(g)$, as might be expected, although the value for B is constant. The constant B value reflects the fact that the data traces run approximately parallel after a time of 150 s.

9. Concluding remarks

The last 10 years have seen significant development of the RAS technique. Its sensitivity to surface dimer orientation and reconstruction, but lack of theoretical understanding, initially led some to view it merely as a weaker substitute for RHEED in environments, such as MOVPE, where RHEED could not operate. Although this was no mean technological

advance in itself, its application in a much wider range of experimental systems coupled with a much improved theoretical understanding now place RAS as a fully fledged surface analytical technique. As has been demonstrated in this article, its range of application is remarkable, having been used to obtain quantitative data on surface chemistry and ordering processes, as well as information on the electrical properties of delta-doped structures and, in conjunction with theory, to actually make predictions of detailed surface structures.

Finally, whilst what may now be termed conventional RAS measurements are carried out with large optical spot sizes on the sample (typically 5 mm in length), it is worth noting that, in a new innovation, Koopmans *et al* have recently carried out microscopic RAS measurements, using a sub-micron spot [77]. They used this technique to determine the in-plane anisotropy of GaAs/AlAs multiple-quantum-well structures, at energies both below and above the fundamental band gap. Confinement and local field effects were discussed, and a comparison made with microscopic calculations based on a tight-binding Hamiltonian for the electronic states.

Acknowledgments

It is a great pleasure to acknowledge the debt we owe to all our co-workers on various RAS projects: David Woolf, Stephen Morris, Julian Bass and Martin Elliott at the University of Wales Cardiff; Frank Reinhardt, Jens Rumberg, Kai Rose, Lisa Steimetz, Thomas Zettler and Wolfgang Richter at Technische Universität Berlin; Jing Zhang, Anna Lees and Bruce Joyce at the IRC for Semiconductor Materials, Imperial College; and Peter Parbrook, Krikor Ozanyan, Mark Hopkinson and Colin Whitehouse at the IRC for Semiconductor Materials and Department of Electronic and Electrical Engineering, University of Sheffield.

We are grateful for financial assistance from the UK Engineering and Physical Sciences Research Council, and from the European Community under the EPIOPTIC and EASI programmes.

References

[1] Aspnes D E, Harbison J P, Studna A A and Florez L T 1987 *Phys. Rev. Lett.* **59** 1687
[2] Aspnes D E, Harbison J P, Studna A A and Florez L T 1988 *J. Vac. Sci. Technol.* A **6** 1327
[3] McGilp J F 1993 *Appl. Surf. Sci.* **63** 99
[4] McGilp J F 1995 *Prog. Surf. Sci.* **49** 1
[5] Morris S J 1994 *PhD Thesis* University of Wales
[6] Zettler J-T 1996 *Prog. in Crystal Growth and Characterization of Materials* (New York: Pergamon)
[7] Sobiesierski Z and Westwood D I 1997 *Thin Solid Films, Proc. European Materials Research Society Meeting (Strasbourg, 1997)* at press
[8] Westwood D I, Woolf D A and Williams R H 1989 *J. Crystal Growth* **98** 782
[9] Wassermeier M, Kamiya I, Aspnes D E, Florez L T, Harbison J P and Petroff P M 1991 *J. Vac. Sci. Technol.* B **9** 2263
[10] Kamiya I, Aspnes D E, Florez L T and Harbison J P 1992 *Phys. Rev.* B **46** 15 894
[11] Ploska K, Zettler J-T, Richter W, Jönsson J, Reinhardt F, Rumberg J, Pristovsek M, Zorn M, Westwood D and Williams R H 1994 *J. Crystal Growth* **145** 44
[12] Zorn M, Trepk T, Zettler J-T, Meyne C, Knorr K, Wethkamp Th, Richter W, Junno B, Miller M and Samuelson L *Proc. 8th Int. Conf. on InP and Related Mater. (Schwabisch-Gmund, 1996)*
[13] Sung M M, Kim C, Bu H, Karpuzov D S and Rabalais J W 1995 *Surf. Sci.* **322** 116
[14] Ozanyan K B, Parbrook P J, Hopkinson M, Whitehouse C R, Sobiesierski Z and Westwood D I 1997 *J. Appl. Phys.* **82** 474
[15] Parbrook P J, Ozanyan K B, Hopkinson M, Whitehouse C R, Sobiesierski Z and Westwood D I 1997 *Proc. 6th Int. Conf. on the Formation of Semiconductor Interfaces (Cardiff, 1997)*

[16] Rose K C, Morris S J, Westwood D I, Woolf D A, Williams R H and Richter W 1995 *Appl. Phys. Lett.* **66** 1930
Morris S J, Zettler J-Th, Rose K C, Westwood D I, Woolf D A, Williams R H and Richter W 1995 *J. Appl. Phys.* **77** 3115
[17] Zorn M, Jönsson J, Krost A, Richter W, Zettler J-T, Ploska K and Reinhardt F 1994 *J. Crystal Growth* **145** 53
[18] Manghi F, Del Sole R, Selloni A and Molinari E 1990 *Phys. Rev.* B **41** 9935
[19] Morris S J, Bass J M and Matthai C C 1995 *Phys. Rev.* B **52** 16 739
[20] Shkrebtii A I and Del Sole R 1993 *Phys. Rev. Lett.* **70** 2645
[21] Kipp L, Biegelsen D K, Northrup J E, Swartz L E and Bringans R D 1996 *Phys. Rev. Lett.* **76** 2810
[22] Kress C, Shkrebtii A and Del Sole R 1997 *Surf. Sci.* **377** 398
[23] Anyele H and Matthai C C 1996 *J. Phys.: Condens. Matter* **8** 6585
[24] Morris S J, Bass J M, Matthai C C, Milman V and Payne M C 1994 *J. Vac. Sci. Technol.* B **12** 2684
[25] Northrup J E and Froyen S 1994 *Phys. Rev.* B **50** 2015
[26] Bass J M and Matthai C C 1996 *J. Vac. Sci. Technol.* B **14** 3075
[27] Esser N, Shkrebtii A I, Resch-Esser U, Springer C, Richter W, Schmidt W G, Bechstedt F and Del Sole R 1996 *Phys. Rev. Lett.* **77** 4402
[28] Mochan W L and Barrera R G 1985 *Phys. Rev. Lett.* **55** 1192
[29] Fahy M R, Ashwin M J, Harris J J, Newman R C and Joyce B A 1992 *Appl. Phys. Lett.* **61** 1805
[30] Wassermeier M, Behrend J, Däweritz L and Ploog K 1995 *Phys. Rev.* B **52** R2269
[31] Woolf D A, Rose K C, Rumberg J, Westwood D I, Reinhardt F, Morris S J, Richter W and Williams R H 1995 *Phys. Rev.* B **51** 4691
[32] Avery A R, Sudijono J, Holmes D M, Jones T S and Joyce B A 1995 *Appl. Phys. Lett.* **66** 3200
[33] Levermann A H, Woolf D A, Westwood D I and Macdonald J A 1996 *Surf. Sci.* **352** 812
[34] Woolf D A, Rose K C, Morris S J, Westwood D I, Rumberg J, Reinhardt F, Richter W and Williams R H 1995 *J. Crystal Growth* **150** 197
[35] Knorr K, Rumberg A, Zorn M, Meyne C, Trepk T, Zettler J-T, Richter W, Kurpas P and Weyers W 1996 *Proc. 8th Int. Conf. on InP and Related Mater. (Schwabisch-Gmund, 1996)*
[36] Davies G J, Heckingbottom R, Ohno H, Wood C E C and Calawa A R 1980 *Appl. Phys. Lett.* **37** 290
[37] Moison J M, Bensoussan M and Houzay F 1996 *Phys. Rev.* B **34** 2018
[38] Hollinger G, Gallet D, Gendry M, Santinelli C and Viktorovitch P 1990 *J. Vac. Sci. Technol.* B **8** 832
[39] Sobiesierski Z, Clark S A, Williams R H, Tabata A, Benyattou T, Guillot G, Gendry M, Hollinger G and Viktorovitch P 1991 *Appl. Phys. Lett.* **58** 1863
[40] Kobayashi N and Kobayashi Y 1992 *J. Crystal Growth* **124** 525
[41] Aspnes D E, Tamargo M C, Brasil M J S P, Nahory R E and Schwarz S A 1994 *J. Vac. Sci. Technol.* A **12** 1180
[42] Kurpas P, Jönsson J, Richter W, Gutsche D, Pristovsek M and Zorn M 1994 *J. Crystal Growth* **145** 36
[43] Jönsson J, Reinhardt F, Zorn M, Ploska K, Richter W and Rumberg J 1994 *Appl. Phys. Lett.* **64** 1998
[44] Sobiesierski Z, Westwood D I, Parbrook P J, Ozanyan K B, Hopkinson M and Whitehouse C R 1997 *Appl. Phys. Lett.* **70** 1423
[45] Esser N, Santos P V, Kuball M, Cardona M, Arens M, Pahlke D, Richter W, Stietz D, Schaefer J A and Fimland B O 1995 *J. Vac. Sci. Technol.* B **13** 1666
[46] Yasuda T, Aspnes D E, Lee D R, Bjorkman C H and Lucovsky G 1994 *J. Vac. Sci. Technol.* A **12** 1152
[47] Aspnes D E 1976 *Optical Properties of Solids: New Developments* ed B O Seraphin (Amsterdam: North-Holland) p 799
[48] Yasuda T, Mantese L, Rossow U and Aspnes D E 1995 *Phys. Rev. Lett.* **74** 3431
[49] Chadi D J 1979 *Phys. Rev. Lett.* **43** 43
[50] Chadi D J 1987 *Phys. Rev. Lett.* **59** 1691
[51] Swartzentruber B S, Kitamura N, Lagally M G and Webb M R 1993 *Phys. Rev.* B **47** 13 432
[52] Cole R J, Tanaka S, Gerber P, Power J R, Farrell T and Weightmann P 1996 *Phys. Rev.* B **54** 13 444
[53] Rossow U, Mantese L and Aspnes D E 1996 *J. Vac. Sci. Technol.* B **14** 3070
[54] Turner A R, Pemble M E, Fernandez J M, Joyce B A, Zhang J and Taylor J G 1995 *Phys. Rev. Lett.* **74** 3213
[55] Zhang J, Taylor A G, Lees A K, Fernandez J M, Joyce B A, Raisbeck D, Shukla N and Pemble M E 1996 *Phys. Rev.* B **53** 10 107
[56] Xie M H, Zhang J, Lees A K, Fernandez J M and Joyce B A 1996 *Surf. Sci.* **367** 231
[57] Liehr M, Greenlief C M, Offenberg M and Kasi S R 1990 *J. Vac. Sci. Technol.* A **8** 2960
[58] Sinniah K, Sherman M G, Lewis L B and Weinberg W H 1989 *Phys. Rev. Lett.* **62** 567
[59] Lees A K, Zhang J, Sobiesierski Z, Taylor A G, Xie M H, Joyce B A and Westwood D I 1996 *Proc. 23rd Int. Conf. on the Physics of Semiconductors (Berlin, 1996)* ed. M Scheffler and R Zimmermann (Singapore: World Scientific) p 955

[60] Zhang J, Lees A K, Taylor A G, Xie M H, Joyce B A, Sobiesierski Z and Westwood D I 1997 *Proc. MBE 9 J. Crystal Growth*
[61] Zhang J 1996 private communication
[62] Power J R, Farrell T, Gerber P, Chandola S, Weightman P and McGilp J F 1996 *Appl. Phys. Lett.* **69** 176
[63] Sobiesierski Z, Westwood D I and Woolf D A 1996 *J. Vac. Sci. Technol.* B **14** 3065
[64] Tanaka H, Colas E, Kamiya I, Aspnes D E and Bhat R 1991 *Appl. Phys. Lett.* **59** 3443
[65] Acosta-Ortiz S E and Lastras-Martinez A 1989 *Phys. Rev.* B **40** 1426
[66] Ashwin M J, Fahy M, Harris J J, Newman R C, Sansom D A, Addinall R, McPhail D S and Sharma V K M 1993 *J. Appl. Phys.* **73** 633
[67] Aspnes D E and Studna A A 1983 *Phys. Rev.* B **27** 985
[68] Sobiesierski Z, Westwood D I and Elliott M 1997 *Phys. Rev.* B at press
[69] Kuball M, Kelly M K, Cardona M, Kohler K and Wagner J 1994 *Phys. Rev.* B **49** 16 569
[70] Houzay F, Guille C, Moison J M, Henoc P and Barthe F 1987 *J. Crystal Growth* **81** 67
[71] Steimetz E, Zettler J-T, Richter W, Westwood D I, Woolf D A and Sobiesierski Z 1996 *J. Vac. Sci. Technol.* B **14** 3058
[72] Steimetz E, Schienle F, Zettler J-T, Richter W, Westwood D, Sobiesierski Z, Matthai C, Junno B, Miller M and Samuelson L 1996 *Proc. 23rd Int. Conf. on the Physics of Semiconductors (Berlin, 1996)* ed M Scheffler and R Zimmermann (Singapore: World Scientific) p 1297
[73] Steimetz E, Schienle F, Zettler J-T and Richter W 1997 *J. Crystal Growth* **170** 208
[74] Yasuda T, Kuo L H, Kimura K, Miwa S, Jin C G, Tanaka K and Yao T 1996 *J. Vac. Sci. Technol.* B **14** 3052
[75] Moison J M, Houzay F, Barthe F, Leprince L, André E and Vatel O 1994 *Appl. Phys. Lett.* **64** 196
[76] Westwood D I unpublished
[77] Koopmans B, Richards B, Santos P, Eberl K and Cardona M 1996 *Appl. Phys. Lett.* **69** 782